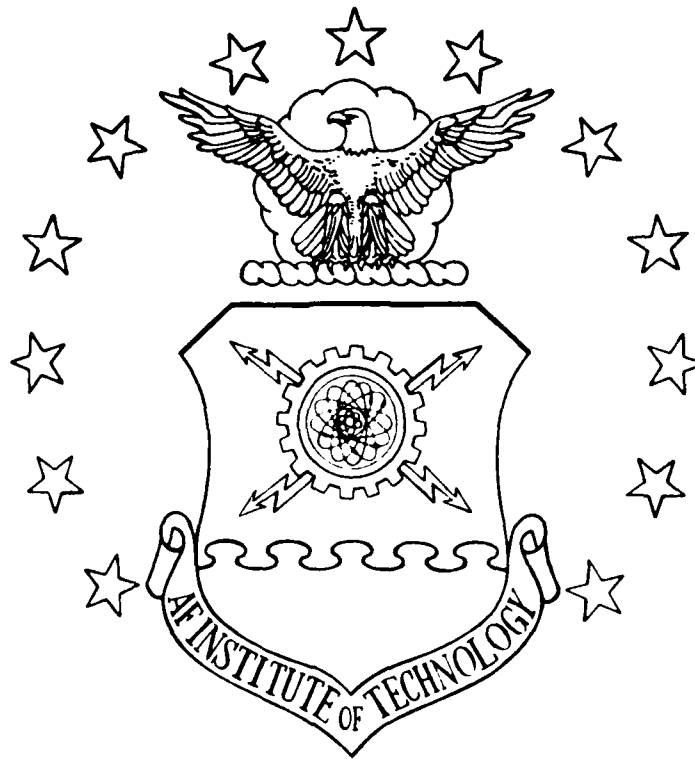AD-A152 114

EXPERIMENTAL INVESTIGATION OF THE PULSED
PHOTOACOUSTIC EFFECT PRODUCED
ON A SOLID SURFACE

THESIS

Haksoo Yoon
Major, ROKAF

AFIT/GEO/PH/84D-6

DEPARTMENT OF THE AIR FORCE

AIR UNIVERSITY

AIR FORCE INSTITUTE OF TECHNOLOGY

DTIC FILE COPY

Wright-Patterson Air Force Base, Ohio

85   03   13   145

EXPERIMENTAL INVESTIGATION OF THE PULSED
PHOTOACOUSTIC EFFECT PRODUCED
ON A SOLID SURFACE

THESIS

Haksoo Yoon
Major, ROKAF

AFIT/GEO/PH/84D-6

AFIT/GEO/PH/84D-6

EXPERIMENTAL INVESTIGATION OF THE PULSED PHOTOACOUSTIC EFFECT

PRODUCED ON A SOLID SURFACE

THESIS

Presented to the Faculty of the School of Engineering

of the Air Force Institute of Technology

Air University

In Partial Fulfillment of the

Requirements for the Degree of

Master of Science

Haksoo Yoon, B.S.

Major, ROKAF

December 1984

Preface

The purpose of this study was to gain an understanding of the characteristics of photoacoustic signals generated at the surfaces of condensed materials. The results of a systematic study of the sound generation mechanism, the propagation characteristics of the sound, and the effects of different materials upon sound production are reported in this thesis. These data are required in the development of non-contact flame thermometry measurements.

For this research the model for peak pressure of a photoacoustic signal, developed by Patel and Tam for liquids, was employed. Several aspects of the model were verified for solids including the dependence of the peak sound pressure upon the radial displacement from the surface, the pump-laser power level, the absorption coefficient, and the specific heat of the material. Numerous material samples were examined for sound production qualities. For measurements of sound pressure, the photoacoustic deflection spectroscopy technique which makes use of a HeNe laser was employed throughout the research.

In performing the experiments and writing this thesis, I have had a great deal of help from others. I am deeply indebted to my sponsor, Dr. Larry P. Goss, for his guidance throughout this project. I also wish to thank my thesis advisor, Prof. Won B. Roh, for his continuous interest, support, and guidance. A word of thanks goes also to Mr. Darryl Trump for his help on equipment preparations and to Mrs. Marian Whitaker for preparation of the manuscript and help with the

illustrations. Finally, I wish to thank my wife Hyekyung for her deep
understanding and concern on those many nights when I was tied to my
desk.

Haksoo Yoon

Table of Contents

List of Figures

List of Tables

AFIT/GEO/PH/84D-6

Abstract

The purpose of this investigation was to determine the character-istics of the photoacoustic signal generated from the surface of a solid material. The important characteristics considered were the dependence of the signal upon 1) the pump-laser power level, 2) the absorption coefficient and specific heat of the material, 3) the radial and axial sound distribution, and 4) the sound distribution with laser focal characteristics.

The model of peak sound pressure for the photoacoustic effect employed in this study was developed by Patel and Tam for liquids. The divergence angles of cylindrical and spherical sound waves were calcu-lated by means of the lateral sound pressure distribution. The optimum sound-producing material was determined by investigating numerous material samples. Throughout the study the peak pressure of the photo-acoustic sound pulse was measured through the use of the linear deflec-tion of a HeNe probe beam.

The results of this investigation indicate that the Patel model for the peak pressure of a photoacoustic signal gives an adequate description of the dependence of the sound pressure upon radial dis-tance and pump-laser power level. However, the dependence of the sound pressure upon the absorption coefficient and the specific heat of a material could not be verified due to the unavailability of absorption

coefficients of the materials studied at the Nd:YAG laser frequency. The results of this study indicate that a cylindrical wave generated by titanium is optimum for applications to the measurement of flame temperatures. The dependence of the sound pressure upon the pump-laser pulse width was not studied.

EXPERIMENTAL INVESTIGATION OF THE PULSED PHOTOACOUSTIC EFFECT PRODUCED ON A SOLID SURFACE

I. Introduction

Background

In 1880, Alexander Graham Bell discovered that when a periodically interrupted beam of sunlight shines on a solid in an enclosed cell, an audible sound can be heard by means of a hearing tube attached to the cell. Subsequent to Bell's discovery, Tyndall and Röntgen showed that an acoustic signal can also be produced when a gas in an enclosed cell is illuminated with chopped light. Bell's subsequent experiments, reported in 1881, with a variety of solids, liquids, and gases generated a brief flurry of interest. The photoacoustic effect, however, was regarded as a curiosity of no practical value and was soon forgotten. Fifty years later the photoacoustic or optoacoustic effect of gases was re-examined. It has since become a well-established technique for gas analysis and is well understood. Photons absorbed by the gas are converted to kinetic energy, giving rise to pressure fluctuations within the cell.

The photoacoustic effect with solids was ignored for more than 90 years; however, about 10 years ago, interest in this effect was revived with its development as a useful technique for spectroscopic investigation of solid and semisolid materials (1:305-308; 2:657-658; 3:548-549; 4:592A-604A). A satisfactory explanation for the effect in solids has

1

been developed, and the name has been changed from optoacoustic to photoacoustic to reduce confusion with the acousto-optic effect by which a laser beam is deflected by acoustic waves in a crystal.

In photoacoustic spectroscopy [PAS] of solids, the sample to be studied is placed inside a closed cell containing a gas, such as air, and a sensitive gas-phase microphone. The sample is then illuminated with chopped monochromatic light. The analog signal from the microphone is amplified and recorded as a function of the wavelength of the incident light. In this way photoacoustic spectra are obtained which correspond to the optical absorption spectra of the solids.

The field of photoacoustic spectroscopy of condensed matter has undergone tremendous growth in the last ten years. Hordvik (5:2877-2833; 6:101-107; 7:2919-2924), Robin (8:131-138; 9:4822-4825), Rosencwaig(1:305-308; 4:592A-604A; 10:1133-1137; 11:64-69), and Samoano (12:128-134) have reviewed various aspects of the field, and Pao (13) has edited a book on the subject. Analytical studies of the dependence of the signal upon chopping frequency, absorption coefficient, and thermal properties have been carried out, for example, by Rosencwaig and Gersho (11:64-69), Aamodt and coworkers (14:927-933; 15:3502-3509; 16:3036-3045), and McDonald and Wetsel (17:2313-2322). However, the gas-phase microphone technique for _ordensed samples relies upon inefficient thermal diffusion into the gas and can be viewed actually as a photothermal technique rather than a photoacoustic one since the acoustic signal generated in the sample plays only a minor role. Thus, this technique has low sensitivity.

In 1979 Patel and Tam (18:467-470) demonstrated a highly sensitive pulsed photoacoustic spectroscopy technique involving the use of pulsed

lasers, a piezoelectric transducer in direct contact with the liquid sample, and a gated detector. This technique provided the first truly photoacoustic measurement because the original acoustic pulse generated in the condensed sample was directly detected by a piezoelectric transducer.

Photoacoustic techniques have recently received attention in the area of combustion diagnostics, where the goal is to understand the basic fluid and chemical properties of combustion. Newly developed combustion-diagnostic techniques which have high sensitivity to minor flame species include photoacoustic spectroscopy (19:118-120; 20:2133-2140), photoacoustic-deflection spectroscopy [PADS] (21:781-784), and photothermal-deflection spectroscopy [PTDS] (22:2663-2665; 23:1333-1344).

One of the interesting applications of the photoacoustic technique is the non-contact flame temperature measurement, which was first demonstrated by Zapka, Pokrowsky, and Tam (24:477-479) in 1982. In this method an intense sound pulse was generated by a plasma spark created by focusing an intense 1064-nm, 10-ns Nd:YAG laser. Two probe beams were employed to monitor the speed of the sound pulse over a distance defined by the probe-beam separation. Since the velocity of sound varies linearly with the square root of the temperature, the temperature can be determined from the sound transit time.

Earlier this year, Kizirnis, Brecha, Ganguly, Goss, and Gupta (25:3873-3881) employed a small wire for sound production as an alternative to sound generation by gas breakdown. This is preferable since the spark blast wave generated by the gas breakdown can greatly disrupt the flow and, in the case of unburnt fuel and air mixture, can even

3

lasers, a piezoelectric transducer in direct contact with the liquid sample, and a gated detector. This technique provided the first truly photoacoustic measurement because the original acoustic pulse generated in the condensed sample was directly detected by a piezoelectric transducer.

Photoacoustic techniques have recently received attention in the area of combustion diagnostics, where the goal is to understand the basic fluid and chemical properties of combustion. Newly developed combustion-diagnostic techniques which have high sensitivity to minor flame species include photoacoustic spectroscopy (19:118-120; 20:2133-2140), photoacoustic-deflection spectroscopy [PADS] (21:781-784), and photothermal-deflection spectroscopy [PTDS] (22:2663-2665; 23:1333-1344).

One of the interesting applications of the photoacoustic technique is the non-contact flame temperature measurement, which was first demonstrated by Zapka, Pokrowsky, and Tam (24:477-479) in 1982. In this method an intense sound pulse was generated by a plasma spark created by focusing an intense 1064-nm, 10-ns Nd:YAG laser. Two probe beams were employed to monitor the speed of the sound pulse over a distance defined by the probe-beam separation. Since the velocity of sound varies linearly with the square root of the temperature, the temperature can be determined from the sound transit time.

Earlier this year, Kizirnis, Brecha, Ganguly, Goss, and Gupta (25:3873-3881) employed a small wire for sound production as an alternative to sound generation by gas breakdown. This is preferable since the spark blast wave generated by the gas breakdown can greatly disrupt the flow and, in the case of unburnt fuel and air mixture, can even

3

cause ignition of the gases. Use of a wire target reduced the perturbation of the flame and the requirements for high peak powers. The sound pulse produced with a wire target is of sufficient amplitude to permit thermometry with laser powers as low as 2 mJ/pulse. The lower energy requirement means that the method can be extended to high-frequency thermometry since low-power high-repetition-rate lasers exist today which can be employed for this purpose. This is extremely important in the study of turbulence and the effects of turbulence upon combustion chemistry since measurements can be made which track the temperature change with time. Presently only 10-30 Hz nonintrusive laser-based techniques are available for thermometry.

This thesis study was conducted specifically to verify the sound-production mechanisms of solid target materials by focused laser sources in order to extend the capabilties of acoustic-based diagnostic techniques. By conducting a systematic study of the sound-generation mechanisms, the propagation characteristics of the sound pulse and the effect of varying the target material can be determined, the optimum target material can be found, the optimum configuration for maximum spatial resolution can be realized, and the diagnostic techniques based on acoustic propagation can be further developed.

Although Kizirnis used a wire target as a sound source, a systematic study of the sound-generation mechanism, the propagation characteristics of the sound, or the effect of different materials on sound production was not conducted. By verifying the present theory of photoacoustic signal generation and investigating the characteristics of the sound pulses, this technique can be further developed.

4

Objective and Approach

The main purpose of this study was to test the model developed by Patel and Tam (26:518-522) for predicting the peak sound pressure generated by high-power Q-switched lasers. Since this model was developed for liquids and has not been tested for solid materials, this study was undertaken to evaluate the applicability of the model for solids. By using the photoacoustic-deflection-spectroscopy technique, the peak amplitudes of the sound pulses were measured under a variety of conditions. Since the measured values were not calibrated, all the values of the peak amplitudes of the sound pulses are relative. In particular, the model was tested for the dependence of the sound pressure upon the radial distance, the pump-laser power, the absorption coefficients, and the specific heats of the target materials used for sound production. Since the pulse width of the Nd:YAG laser was fixed, the dependence upon the pulse width of the pump laser could not be studied. Although the model was developed specifically for the case of cylindrical sound propagation from a line source, the case of spherical sound propagation was examined also.

Other important experiments which were conducted include amplitude distributions of the spherical and cylindrical sound waves and selection of the optimum material for sound generation. These experiments are important to the photoacoustic-deflection thermometry technique because of spatial-resolution requirements and need for materials which can produce large sound peaks with minimum laser power and withstand flame temperatures.

II. Theory

Photoacoustic Signal Generation

Numerous investigators have studied the problem of photoacoustic signal generation in a liquid or in a solid arising from the absorption of a light beam. Most studies treated the case of surface heating by a pulsed laser [for example, Askarayan and co-workers (27:1463-1465), Bell and Landt (28:46-68), Bushanam and Barnes (29:2074-2082), Emmony and co-workers (30:547-549), Gordienko and co-workers (31:73-74), Gournay (32:1322-1330), Von Gutfeld and Budd (33:617-619), Sigrist and Kneubühl (34:1652-1663), and White (35:3558-3567)]. Other investigators (36:67-71; 13:193-238) have treated the case of the steady-state solution for a sinusoidally modulated light beam in such a way that all time-varying quantities have the $\exp(i\omega t)$ form. These studies were followed by those of Patel and Tam who were primarily interested in the case where the time-dependent signal is due to pulsed excitation with low optical absorption (i.e., a sample that is highly transparent to light). Although this research was not directly related to transparent material such as water, the equation for the sound signal generated by a solid and propagated through air was verified. Their work is most directly related to the use of pulsed photoacoustic spectroscopy for measuring weak absorption in condensed matter. This case has been treated by a few investigators (37:98-99; 38:3348-3358) with varying degrees of mathematical rigor. It is interesting that in each of the three different cases mentioned above (surface absorption of a pulsed laser, steady-state solution for a sinusoidally modulated light beam,

6

and weak bulk absorption of a pulsed laser), the solution is character-
ized by the following form:

$$\frac{P_0}{E_0} = \text{const}\ \frac{\beta v_a \alpha}{C_p} \tag{1}$$

where P_0 is the acoustic pressure amplitude developed, E_0 is the laser
energy per pulse or per cycle, β is the thermal expansion coefficient,
C_p is the specific heat at constant pressure, v_a is acoustic velocity,
and α is the optical absorption coefficient of the medium. The case of
weak bulk absorption of a pulsed laser beam will now be considered in
greater detail.

Consider a thin cylinder of a liquid, illustrated in Fig. 1 (or
solid if only longitudinal waves are considered), of length ℓ and opti-
cal absorption coefficient α, irradiated by a laser pulse of duration
$\tau_p = 2\tau$ and pulse energy E_0. The case of weak absorption, i.e.,
$\alpha\ell \ll 1$, where the absorbed energy $E_0\alpha\ell$ is distributed uniformly along
the length ℓ, is of primary interest in this theory. In this case the
weak absorption results in a cylindrical wave produced by the thin
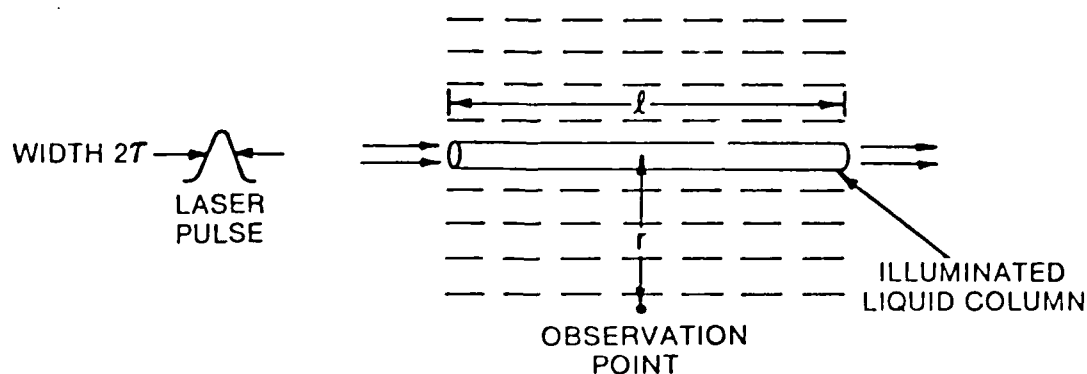
Figure 1. Theoretical Calculation of the Pulsed PA Effect

7

cylindrical volume. Here, the acoustic pressure $P(r,t)$ at an observation point is examined as a function of the radial distance r and time t. Since the acoustic source is assumed to be a long thin cylinder, the only spatially dependent variable is r.

Phenomenological Description of PA Signal Generation. The generation of a photoacoustic signal relies upon the conversion of absorbed optical radiation into heat through nonradiative relaxation processes. Rigorous derivation of acoustic pulse generation following the absorption of a pulsed beam of optical radiation is described in the next section. The phenomenological description, which will be given here, contains most of the physics underlying photoacoustic signal generation. The key parameter is the rapid conversion of the absorbed energy into heat by nonradiative relaxation processes. Figure 1 shows schematically a laser beam of radius R traveling in a cell containing a piezoelectric transducer. It is assumed that the laser pulse length τ_p is much longer than the nonradiative relaxation time τ_{NR} and the time τ_a required for an acoustic pulse to travel across the laser-illuminated region in the liquid, i.e.,

$$\tau_p \gg \tau_{NR} \qquad (2)$$

$$\tau_p \gg \frac{2R}{v_a} \equiv \tau_a \qquad (3)$$

where v_a is the acoustic velocity in the medium. Also the laser pulse is assumed to be much longer than the response time of the piezoelectric transducer, τ_{pzt}, i.e.,

$$\tau_p \gg \tau_{pzt} \qquad (4)$$

8

Under these conditions the energy absorbed by the medium having absorption coefficient α and length ℓ is given by

$$E_{abs} = E_0(1 - e^{-\alpha\ell}) \tag{5}$$

where E_0 is the input laser pulse energy. For $\alpha\ell \ll 1$, a situation to be examined,

$$E_{abs} \sim E_0\alpha\ell \tag{6}$$

Since it is assumed that nonradiative relaxation predominates in the medium, the thermal energy E_{th} is given by

$$E_{th} = E_{abs} = E_0\alpha\ell \tag{7}$$

Knowing the specific heat at constant pressure C_p, the temperature rise ΔT of the illuminated volume can be evaluated from

$$E_{th} = C_p V \Delta T \rho \tag{8}$$

where V is the illuminated volume and ρ is the density of the medium. Since

$$V = \pi R^2 \ell \tag{9}$$

the temperature rise is

$$\Delta T = \frac{E_0\alpha}{\pi R^2 C_p \rho} \tag{10}$$

9

Now if one assumes adiabatic, isobaric expansion, the new volume of the illuminated region can be calculated. With ΔR being the increase in the radius of the illuminated volume,

$$\pi R^2 \ell - \pi(R + \Delta R)^2 \ell = \beta V \Delta T \tag{11}$$

where β is the volumetric expansion coefficient. If $\Delta R \ll R$, the increased radius is

$$\Delta R \sim \frac{1}{2} R \beta \Delta T \tag{12}$$

Inserting ΔT from Eq. (10),

$$\Delta R = \frac{E_0 \alpha \beta}{2 \pi R C_p \rho} \tag{13}$$

This expansion creates a pressure wave which travels radially outward from the illuminated cylinder at the velocity of sound. The change in pressure P created at a point is related to the frequency of the sound wave f_a and the displacement $\Delta \chi$ through

$$P = 2 \pi f_a v_a \Delta \chi \rho \tag{14}$$

But $\Delta \chi$ is proportional to ΔR evaluated in Eq. (12). Thus, $\Delta \chi = \text{const} \times \Delta R$ and

$$P = \text{const.} \frac{f_a}{R} \frac{\beta v_a}{C_p} E_0 \alpha \tag{15}$$

For a fixed geometry of laser illumination and properties, f_a and R are constant. Therefore,

10

$$F = \text{const.} \frac{\beta v_a}{C_p} E_0 \alpha \qquad (16)$$

Since the electrical signal output from a piezoelectric or deflection transducer is given by

$$V_{pa} = \text{const.} \times P \qquad (17)$$

one obtains

$$V_{pa} = K' \frac{\beta v_a}{C_p} E_0 \alpha \qquad (18)$$

where K' is a constant that includes the geometrical parameters as well as the response properties of the piezoelectric transducer. Then, the normalized photoacoustic signal S is

$$S = \frac{V_{pa}}{E_0} = K' \frac{\beta v_a}{C_p} \alpha \qquad (19)$$

$$= K\alpha \qquad (20)$$

Thus, a measurement of the normalized photoacoustic signal for a given material gives direct information regarding the absorption coefficient α. Equation (19) contains most of the important parameters necessary for the practical use of photoacoustic spectroscopy for quantitative measurements of small absorption coefficients in condensed matter, but it does not provide any information regarding the temporal or spatial distribution of the photoacoustic output pulse. The detailed derivation will be discussed below.

11

Rigorous Description of PA Signal Generation. In a more rigorous
treatment of photoacoustic pulse generation, a potential function $\phi(r,t)$
is used to define the acoustic field, with the acoustic velocity V_a and
pressure P given by

$$V_a = \nabla\phi \tag{21}$$

and

$$P = -\rho \frac{\partial\phi}{\partial t} \tag{22}$$

For the case of a long thin cylinder generating an acoustic wave due to
the time-dependent expansion of the cylinder, Landau and Lifshitz
(39:283) have shown that the potential ϕ is given by

$$\phi(r,t) = - \frac{v_a}{2\pi} \int_{-\infty}^{t-(r/v_a)} \frac{\dot{S}(t')dt'}{[v_a^2(t - t')^2 - r^2]^{1/2}} \tag{23}$$

where $\dot{S}(t')$ is the time derivative of the cross-sectional area S(t') of
the cylindrical source at retarded time t', i.e.,

$$\begin{aligned} S(t') &= \pi[R + \Delta R(t')]^2 \\ &\sim \pi R^2 + 2\pi R\Delta R(t') \end{aligned} \tag{24}$$

Here R is the unperturbed radius of the cylindrical source and $\Delta R(t')$ is
the expansion at time t' due to the laser pulse. The value of $\Delta R(t')$ is
always many orders of magnitude smaller than R for cases of interest.

The pressure of the sound pulses will be derived using Eq. (22).
Since the limit of integration in Eq. (23) is t dependent, it is

12

convenient to change variables, using $t'' = [t - t' - (r/v_a)]$ in Eq. (23) before differentiation and then change back to t' after differentiation. Thus, the potential function becomes

$$\phi(r,t) = -\frac{v_a}{2\pi} \int_{-\infty}^{0} \frac{\dot{S}(1 - t'' - \frac{r}{v_a})}{[(v_a t'' + r)^2 - r^2]^{1/2}} \, dt'' \tag{25}$$

and, hence, the pressure P is

$$P(r,t) = \frac{\rho v_a}{2\pi} \int_{-\infty}^{t-(r/v_a)} \frac{\ddot{S}(t) dt'}{[v_a(t - t')^2 - r^2]^{1/2}} \tag{26}$$

By using Eq. (24), the pressure distribution becomes

$$P(r,t) = \frac{\rho v_a}{2\pi} \int_{-\infty}^{t-(r/v_a)} \frac{2\pi R \Delta \ddot{R}(t') dt'}{[v_a^2(t - t')^2 - r^2]^{1/2}} \tag{27}$$

Equation (27) is the basic "causality expression" relating the pressure at the observation point and the time derivative of the velocity of expansion of the source at retarded times.

To proceed further, some simple forms for $\Delta \ddot{R}(t')$ are needed. It is assumed that the time dependence of the pulsed laser irradiation can be approximated by a Gaussian centered at $t'' = 0$, with width 2τ and total energy E_0:

13

$$\frac{dE(t')}{dt'} = \frac{E_0}{\pi^{1/2}\tau} e^{-(t'/\tau)^2} \tag{28}$$

where $E(t')$ is the integrated laser energy up to time t' and $E(\infty) = E_0$. When one neglects heat diffusion from the cylindrical source volume during the duration of the laser pulse, the volume expansion of the source at t' goes to

$$\pi[R + \Delta R(t)]^2 - \pi R^2 = \beta\alpha E(t')/(\rho C_p) \tag{29}$$

When the laser pulse is long compared to the acoustic transit time across the cylindrical optical beam in a liquid, the local pressure equilibrium is maintained and one can apply the specific heat at a constant pressure. Heat diffusion is always negligible, since the diffusion length λ_{diff} in a time interval τ is given by

$$\lambda_{diff} = (4\tau D)^{1/2} \tag{30}$$

where D is the thermal diffusivity. By neglecting the $\Delta R^2(t')$ term in Eq. (29), one obtains

$$2\pi R\Delta R(t') \approx \beta\alpha E(t')/(\rho C_p) \tag{31}$$

By combining Eqs. (28) and (31),

$$2\pi R\Delta\ddot{R}(t') = \frac{\beta\alpha}{\rho C_p} \frac{E_0}{\pi^{1/2}\tau} \frac{(-2t')}{\tau^2} e^{-(t'/\tau)^2} \tag{32}$$

14

Substituting this equation into Eq. (27),

$$P(r,t) = - \frac{v_a \beta \alpha E_0}{\pi(\pi)^{1/2} C_p \tau^3} \times \int_{-\infty}^{t-(r/v_a)} \frac{t' e^{-(t'/\tau)^2} dt'}{[v_a^2(t - t')^2 - r^2]^{1/2}} \qquad (33)$$

One may refer to Eq. (33) as the pulsed photoacoustic equation, relating the transient acoustic pressure P at the observation point to the retarded time development of the laser pulse. This equation has the form indicated in Eq.(1), with the "const" containing v_a, τ, and an r-dependent retarded time integral.

Simplification of Eq. (33) is possible for sufficiently large r; therefore, the integrand in Eq. (33) is most important when $t - t' \sim r/v_a$. Hence, one can make the following approximation:

$$v_a^2(t - t')^2 - r^2 \sim 2r[v_a(t - t') - r] \qquad (34)$$

and Eq. (33) becomes

$$P(r,t) = - \frac{v_a \beta \alpha E_0}{\pi(2\pi r)^{1/2} C_p \tau^3} \times \int_{\infty}^{t-(r/v_a)} \frac{t' e^{-(t'/\tau)^2} dt'}{[v_a(t - t') - r]^{1/2}} \qquad (35)$$

In Eq. (32), the source term $\Delta \ddot{R}(t')$ has the largest amplitude at $t' = \pm 0.7\tau$ and vanishes rapidly at large $|t'|$. Thus, P(r,t) has the largest magnitude at $t_{\pm} \sim r/v_a \pm 0.7\tau$. Approximate evaluation of the integral in Eq. (34) shows that

15

$$P(r,t_\pm) \sim \frac{\beta\alpha E_0}{\pi C_p \tau^2} \left(\frac{v_a \tau}{2\pi r}\right)^{1/2} \equiv \pm p_0(r) \qquad (36)$$

This is the equation investigated throughout this study. Several interesting observations are possible with the pressure amplitude predicted in Eq. (36). First, the compression pulse at time t_- is followed by a rarefaction pulse (of nearly equal magnitude) at time t_+, with the time interval between the compression and rarefaction being approximately the laser pulse width. This has been confirmed by several investigators, for example, Bunkin and Komissarov (40:203-211), Lyamshev and Naugol'nykh (41:354-355), and Naugol'nykh (37:98-99). Secondly, the pressure amplitude $P(r,t)$ decreases with distance as $r^{-1/2}$, in accordance with the conservation of energy in cylindrical symmetry, as noted by Landau and Lifshitz. When the source is a point, the pressure amplitude decreases with distance as $1/r$, in accordance with the conservation of energy. The functional dependence of amplitude upon r for both cylindrical and spherical propagation was verified in the present study.

Probe Beam Deflection by PA Signals

Jackson and his coworkers derived the equation for probe beam deflection as a function of the index of refraction (23:1335). They used the index of refraction as a function of temperature and neglected the pressure contribution since, under the conditions of their study, it was very small compared to the temperature contribution. They noted, however, that the pressure contribution to the index of refraction has experimental importance at high frequencies, large probe beam

offsets, and/or high pump beam peak powers, which is the case in the present study. Their derivation is followed here.

The index of refraction as a function of pressure is

$$n(r,t) = n_0 + \Delta n(r,t) = n_0 + \frac{\partial n}{\partial P}\bigg|_{P_{ambient}} P(r,t) \qquad (37)$$

The propagation of the Gaussian probe beam through the spatially varying index of refraction is given by (42:2434)

$$\frac{d}{dS}\left(n_0 \frac{dr_0}{dS_r}\right) = \nabla_\perp n(r,t) \qquad (38)$$

where r_0 is the perpendicular displacement of the beam from its original direction, n_0 is the uniform index of refraction, and $\nabla_\perp r(r,t)$ is the gradient of the index of refraction penpendicular to S_r (the ray path) (Fig. 2). Integrating Eq. (38) over S_r gives

$$\frac{dr_0}{dS_r} = \frac{1}{n_0}\int_{path}\nabla_\perp n(r,t)\ dS_r \qquad (39)$$

$$= \frac{1}{n_0}\frac{\partial n}{\partial P}\int_{path}\nabla_\perp P(r,t)\ dS_r \qquad (40)$$
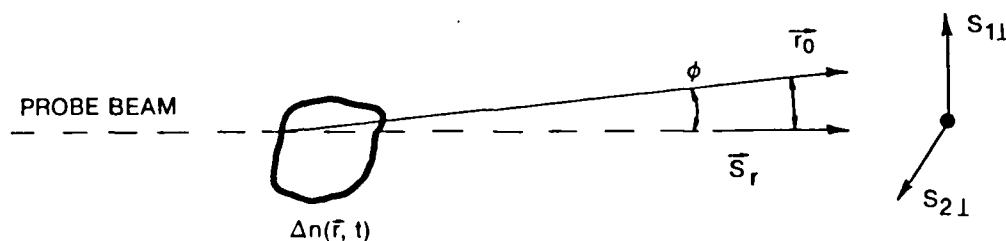
Figure 2. Scattering Geometry. Scattering region may focus the beam differently in the $S_{1\perp}$ and $S_{2\perp}$ directions (elliptical Gaussian beams) (From Ref. 23)

For gases ($n \sim 1$), the index of refraction can be expressed as

$$n - 1 = K_{GD}\rho_{gas} \tag{41}$$

where K_{GD} is the Gladstone-Dale constant and ρ_{gas} is the density of the gas. Equation (41) is known as the simpler Gladstone-Dale law (43:24-16). Since ρ_{gas} is linearly proportional to the pressure of the gas, Eq. (41) becomes

$$n - 1 = KP \tag{42}$$

Therefore,

$$\frac{\partial n}{\partial P} = K \tag{43}$$

From Eq. (41),

$$\frac{dr_o}{dS_r} = K' \int_{path} \nabla_\perp P(r,t) \, dS_r \tag{44}$$

since n_o and $\partial n/\partial p$ are constant. When the path is the same for all measurements,

$$\frac{dr_o}{dS_r} = K'' P(r,t) \tag{45}$$

Equation (45) indicates that the displacement of the probe beam from its original direction is linearly proportional to the sound pressure.

Detector Response

Deflection of the probe beam due to a change in the index of refraction is detected by a position-sensitive detector which converts the deflection into an output voltage. The change in the signal ΔV_{det} above the dc level V_{det} is demonstrated in Fig. 3. Assuming a Gaussian probe beam,

18
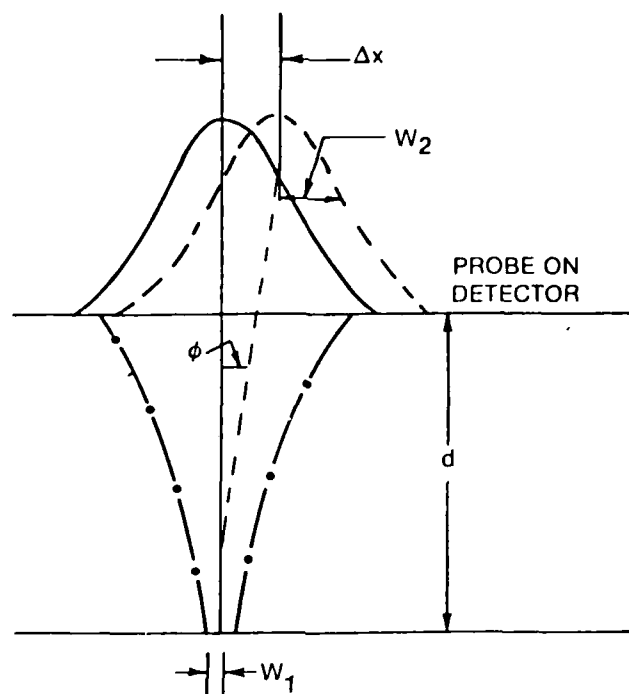
Figure 3. Probe Spot on Detector

$$\frac{\Delta V_{det}}{V_{det}} = \frac{\Delta I}{I_0} \approx 4\Delta x \int_0^\infty \frac{2}{\pi w_2^2} \ \exp \ (-2r^2/w_2^2) dr$$

$$\approx (\frac{4}{\sqrt{2\pi}}) \ \frac{\Delta x}{w_2} \tag{46}$$

where $\Delta x = \phi d$, d is the distance from the focal spot to the detector, I_0 is the probe beam intensity, and w_2 is the spot radius on the detector. Since d is large,

$$w_2 \sim (\lambda d)/(\pi w_1 \ n_0) \tag{47}$$

where w_1 is the probe beam radius at the focal spot, λ is the probe beam wavelength, and n_0 is the index of refraction of the air. Hence,

$$\nabla V_{det} = \frac{4}{\sqrt{2\pi}} \ \frac{\phi \pi w_1 n_0}{\lambda} \ V_{det} \tag{48}$$

19

However, $\phi \sim dr_0/dS_r$, since the deflection is very small. Therefore,

$$\nabla V_{det} \sim \frac{4}{\sqrt{2\pi}} \frac{\pi w_1 n_0}{\lambda} \frac{dr_0}{dS_r} V_{det}$$

$$= K \frac{dr_0}{dS_r} \tag{49}$$

since w_1, n_0, λ, and V_{det} are constant. When the probe beam is not focused, which is the case in the present study, d is the deflected spot distance from the detector and w_1 is the probe beam radius at the deflected spot. When the deflected spot is limited to one position, d and w_1 remain constant; therefore, the voltage change is still a linear function of displacement of the probe beam at the detector.

III. Experimental Apparatus

Pumping Laser Source

A Quanta-Ray DCR pulsed Nd:YAG laser was used as the pumping laser source, with the output beam being focused at the surface of a target material. The specifications of the Nd:YAG laser are listed in Table I. Although the power of the Nd:YAG laser is adjustable, the middle range of operation was used for stability, and most of the powe changes were accomplished through the use of various neutral density filters. The beam profile of this laser has a doughnut rather than a Gaussian shape, and the intensity is nonuniform throughout the cross section of the beam. Therefore, to achieve a line source, the beam was expanded and refocused by means of several concave and convex lenses. Only the Nd:YAG oscillator was used in this experiment since the output pulse energy required to generate a sufficient photoacoustic signal at the target was 6 mJ.

Probe Beam Laser Source

As the probe beam source for detecting photoacoustic signals, the Spectra-Physics Model 105 helium-neon (HeNe) laser with the Model 205 Power Supply was used. Its specifications are listed in Table II.

Position-Sensitive Detector

A Silicon Corporation Model SD-380-23-21 position-sensitive detector was used to detect the deflection of the HeNe beam caused by the photoacoustic signal. This detector has four quadrants; the two oriented in the direction of the deflection were used in the present

TABLE I

Product Specifications of Quanta-Ray

DCR Pulsed Nd:YAG Laser

Parameter	Specification
Wavelength	1,064 nm
Pulse Width	10 nsec.
Pulse Energy	70 mJ/pulse with amp./osc.
Pulse Energy Stability	1%
Beam Diameter	6.4 mm
Beam Divergence	0.5 mrad
Optimum Pulse Repetition Rate	10 pulse/sec.
Output Pulse Time Jitter	< 0.25 nsec r.m.s. from Q-sw sync. pulse
Spatial Mode	Unstable resonator, uniphase, near diffraction limited
Linewidth at 1,064 nm	< 1 cm^{-1}
Average Power Stability	5% per 10 hr.
Beam Pointing Stability	< 0.5 mrad

TABLE II

Product Specification of Spectra-Physics

Model 105 HeNe Laser

Parameter		Specification
Power Output, TEMoo (632.8 nm)		> 5 mW
TEMoo Mode Purity		> 95%
Beam Diameter		0.83 ± 0.02 mm
Beam Divergence		1.0 mrad.
Beam Quality	Random Spatial Noise	< 1%
	A/R Spot Intensity	< 0.25%
Beam Amplitude Noise (20 Hz - 2 MHz)		0.5% rms. max.
Operating Current		6.5 ± 0.1 mA
Operating Voltage		3,460 ± 100 V
Weight		1.94 lb/880 g

experiment. The general structure of the detector is illustrated in Fig. 4. Region 3 detects the amount of deflection of the HeNe probe beam caused by the compression region of the photoacoustic signal, and Region 1 detects the amount caused by the rarefaction region of the signal. The operating specifications at room temperature ($23^{o}C$) are listed in Table III.

Oscilloscope and Digitizer

The output of the position-sensitive detector was observed by a Tektronix Model 7904 oscilloscope equipped with a programmable digitizer
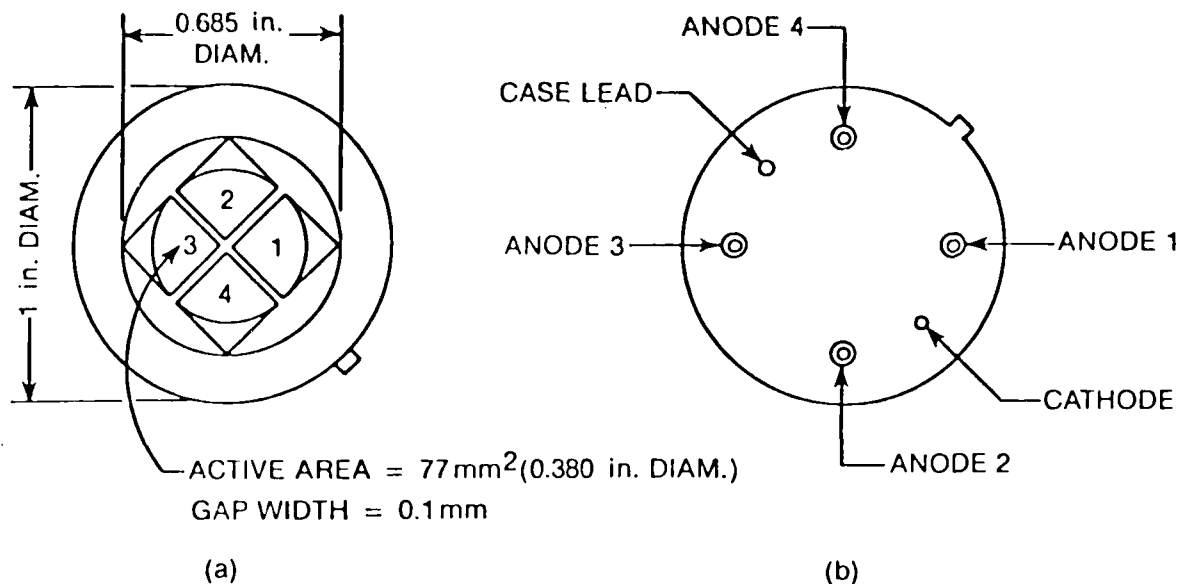
Figure 4.   Structure of the SD-380-23-21 Position-Sensitive
Detector; (a) Top View, (b) Bottom View

(Model 7D20) and triggered by the Q-switch pulse from the Nd:YAG laser.
In most cases the signals from the detector were stored in the digitizer
and averaged over about 250 pulses. Accurate measurements of the dis-
played signal amplitude (referenced to ground) and time (referenced to
trigger position) were made using the internal memory of the digitizer.

Power and Energy Meter

A Scientech Model 362 Power Meter was used to measure the output
energy from the Nd:YAG laser. Its specifications are listed in Table IV.

TABLE III

Operating Specifications of SD-380-23-21

Position-Sensitive Detector

Parameter	Specification
Typical Peak Responsivity	0.55 A/W
Max. Nonuniformity of Response when Scanned with 1-mm Light Spot	±5%
Typical Position Sensitivity at Spectral Peak	0.5 P/R A/cm
Guaranteed Position Measurement Accuracy over Operating Range	± 0.06 R cm for Uniform Spot
Min. Detectable Position Change	$1.5 \sqrt{\Delta f/H}$ Å
Typical Thermal Drift of Null Point	$R \times 10^{-5}$ μm/°C
Measurement Range (Active Area Size)	-R to +R (Dual-Axis) cm
Max. Total Light Current (Sum of Outputs)	10 μA
Max. Total Light Power on Device at Spectral Peak - P	0.18 mW
Max. Light Power Density at Spectral Peak - H	25 mW/cm^2

R ≡ Radius of light spot in cm
P ≡ Total light power on device in W
Δf ≡ System bandwidth in Hz
H ≡ Power density of light spot in W/cm^2

TABLE IV

Product Specifications of Scientech Model 362

Power and Energy Indicator and Sensor

| Parameter	Specification
Laser Power Range	1 mW - 10 W full scale
Laser Energy Range	1 mJ - 10 J full scale
Time Constant of Indicator	4 sec with 3,600 disc. calorimeter (14 sec on 10-W/J range)
Spectral Response	Flat from 0.25 to 35 μm
Accuracy	$\pm$ 3%
Aperture of Sensor	1 in.
Time Constant of Sensor	14 sec
Max. Power Density	500 W/cm^2 CW 1 mW/cm^2 Pulse

IV. Experimental Procedure

Experimental Setup

As shown in Fig. 5, the Quanta Ray DCR pulsed Nd:YAG laser beam was focused at the surface of the target material. The output of the unstable resonator of the Nd:YAG laser is a few times diffraction limited and can be easily focused to a point. However, using the unstable resonator to make a focal line at the surface of the target was very difficult. Several convex and concave spherical and cylindrical lenses were used for this purpose. The most uniform portion of the line source was selected by placing an adjustable aperture after the optical arrangement. The target surface was placed perpendicular to the Nd:YAG beam. The power meter was located behind the target material which was removed when a power measurement was made.

As shown in Fig. 6, the HeNe laser and the position-sensitive detector were mounted on an optical rail which could be moved laterally or radially. The position of the detector was adjusted to achieve the maximum response by means of a translation stage. The detector was apertured to prevent the detection of scattered light from the Nd:YAG beam.

The acoustic wave generated by the absorption of the pump beam at the surface of the target material deflects the probe beam by an amount which is related linearly to the sound pressure (23:1333-1344). Therefore, by measuring the deflection at different points with a position-sensitive detector, one can determine the relative peak pressure of the sounds at those points. The signal from the position-sensitive detector was displayed on the digitizing oscilloscope, as shown in Fig. 7; 250
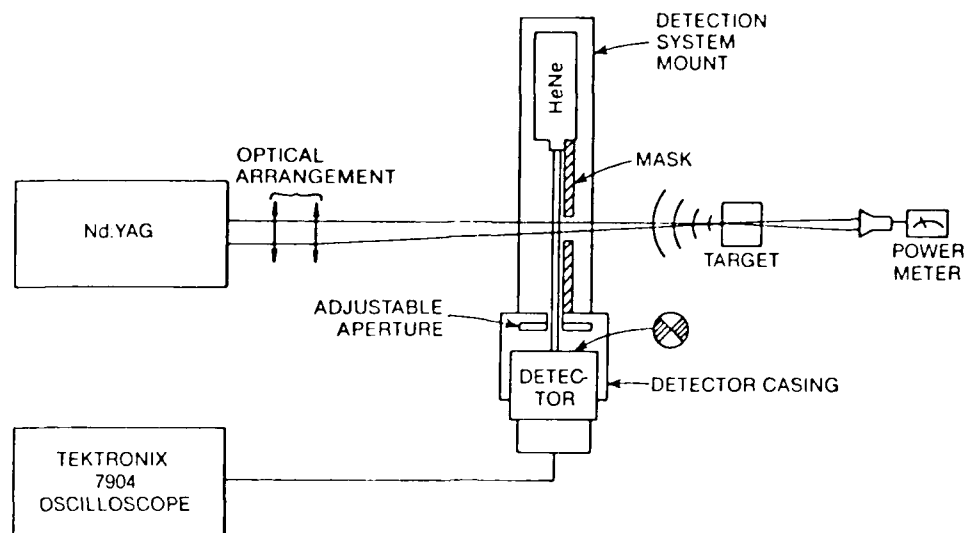
(a)

(b)

Figure 5. Experimental Setup; (a) Schematic
Illustration, (b) Photograph
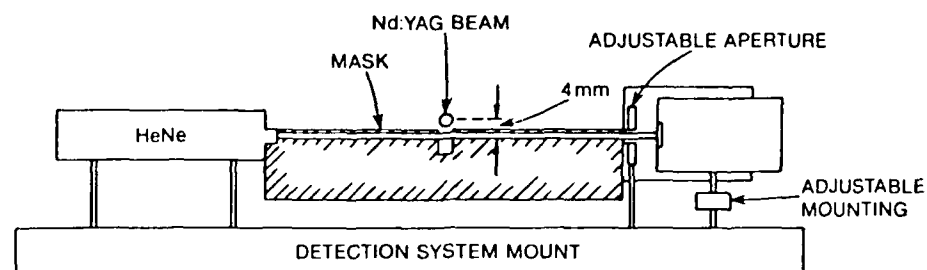
(a)
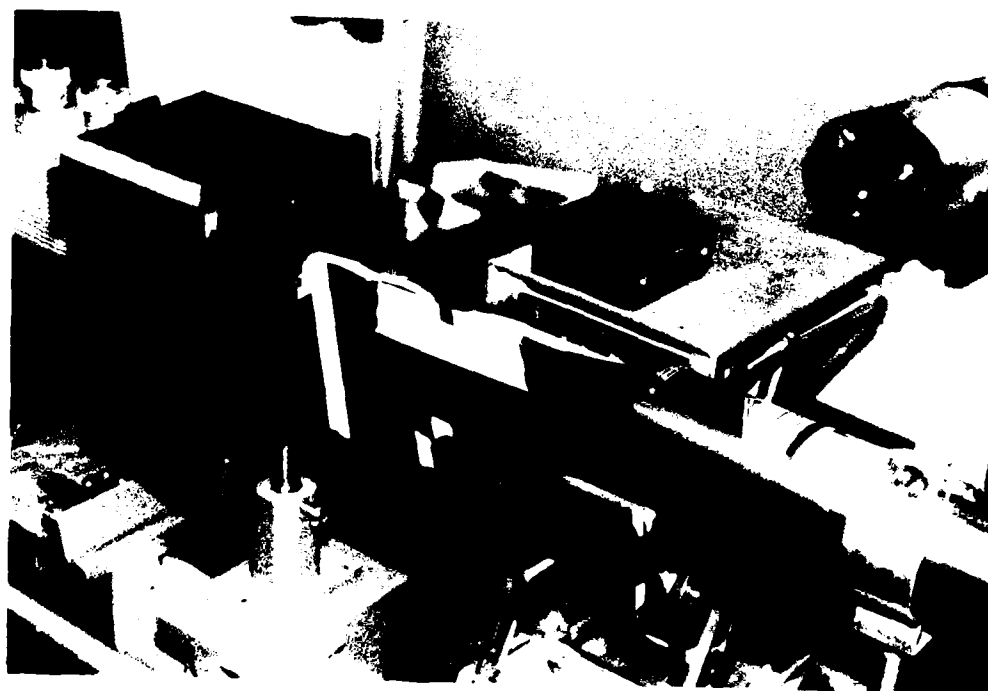
(b)

Figure 6. Detection System; (a) Schematic
Illustration, (b) Photograph
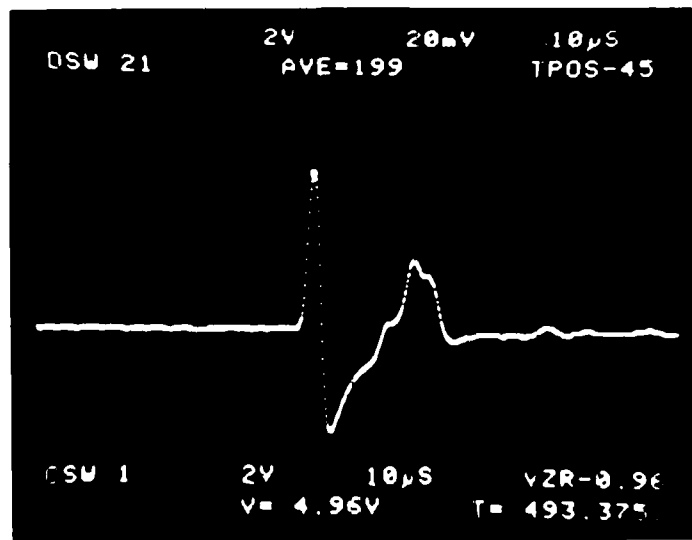
Figure 7. HeNe Probe Beam Deflection
Displayed on Oscilloscope

pulses were stored and averaged by the digitizer at one measurement
point, and this value was normalized to a reference point.

Masking Effect on the Probe Beam

One major drawback of using HeNe laser deflection for measuring the
sound pressure is the fact that this deflection method is a line-of-
sight technique. The index-of-refraction gradient produced by the
intense sound can deflect the beam at any point between the laser source
and position detector. This is a problem when measuring a sound distri-
bution which diverges from the sound source, as is the case with a point
source. If the sound diverges radially, a larger area of the probe beam
is intersected at farther radial positions, resulting in the measured

acoustic signal depending not only upon the pressure amplitude but also upon the intersected area of the probe beam.

The model of Patel and Tam which is used to predict the sound pressure radial distribution does not account for this feature. To circumvent this problem a mask was placed between the sound source and the HeNe probe laser which fixed the area over which the pressure wave interacted with the probe laser. This eliminated the line-of-sight problem, as demonstrated in the results section.

The line-of-sight nature of the deflection technique was not a problem with a cylindrical sound source since the radial divergence of this source is quite small and, thus, the measurement area of the probe beam remains constant.

Verification of Radial Distance Relation of PA Signal

By measuring the amplitudes of the sound pulses at different radial positions, the radial-distance dependence of the sound propagation was verified. This measurement was made for point sources and line sources. Since the amplitude of the sound pulses decreases gradually with time, a reference point was chosen and each measurement was compared with the averaged reference value.

This experiment was performed with and without a mask to confirm the masking effect, and the two sets of data were compared. A steel target was used in this measurement.

Lateral Amplitude Distribution of PA Signal

By moving the detection system laterally, while keeping the radial distance constant, the lateral amplitude distributions of the PA signals for a point source and several line sources were determined. When

moving the detection system laterally, the apparent size of the aperture in the mask changes and the sound pulse does not pass through the probe beam perpendicularly. However, both of these effects were neglected because the radial distance was large and the distance over which the detection system moved was small.

Verification of Pump-Laser Power Dependence

In this experiment the experimental apparatus remained stationary, while the power of the Nd:YAG laser was varied. Each data point was an average of 250 pulses at a given power level. For every subsequent data point, the target was moved axially to eliminate the ill effects of the previous measurements at that spot. A steel target was used for this experiment.

Comparison of Amplitudes of PA Signals Generated by Different Target Materials

In this experiment the target material was varied to compare the sound-generating properties of different metals at a constant Nd:YAG laser power. The amplitude of the sound was measured at 1-min. intervals for 25-30 min., and the amplitude was plotted as a function of time. Since the amplitude of a sound pulse is a linear function of the ratio of the absorption coefficient to the specific heat of the material, the dependence of the sound amplitude upon the value of α/C_p was examined. The PA signals from three different geometries (target located behind, in front of, and well in front of the focus) were measured and compared separately. Only point sources were used for this measurement in order to make the source more uniform and to simplify

calculation of the power density of the Nd:YAG laser beam at the focused region.

The metallic target materials used were (1) stainless steel, (2) steel, (3) titanium, (4) titanium alloy, (5) aluminum, (6) copper, (7) brass, (8) tungsten, and (9) nickel. For nonmetallic target materials, Plexiglas, smoked Plexiglas, graphite, Fiberglas, ZrO_2, and ceramic were employed.

V. Results and Discussion

Verification of the Spherical Propagation of PA Signal

The relative amplitudes of the PA signals generated from a point source were measured at different radial positions. This experiment was performed with and without a mask.

Without Mask. The results of relative amplitude measurements at different radial positions are shown in Fig. 8. The amplitude of the PA signal at downstream positions is slightly higher than the value calculated from a 1/r relation. Without the probe-beam mask which serves to limit the area over which the pressure wave is measured, the downstream radial positions intersect a larger portion of the HeNe probe beam, resulting in a higher measured sound amplitude. By limiting this area the correct radial dependence can be measured, as discussed below.

With Mask. The actual radial-distance relation measured by means of a small aperture is shown in Fig. 8. The radial-distance dependence, which was predicted to be 1/r, was found to be consistent with the experimental results.

At small radial distances (up to 15 cm), an aperture size of 0.7 cm was used; and at large distances (15-35 cm), 1.5 cm was used. The amplitudes measured with the larger aperture were calibrated with those measured with the smaller one. Although the relative amplitudes with and without a mask are shown in one figure, the actual amplitudes differ widely.

A reference point was set at 3 cm from the target for measuring amplitudes at short distances, and each measurement was compared with

34
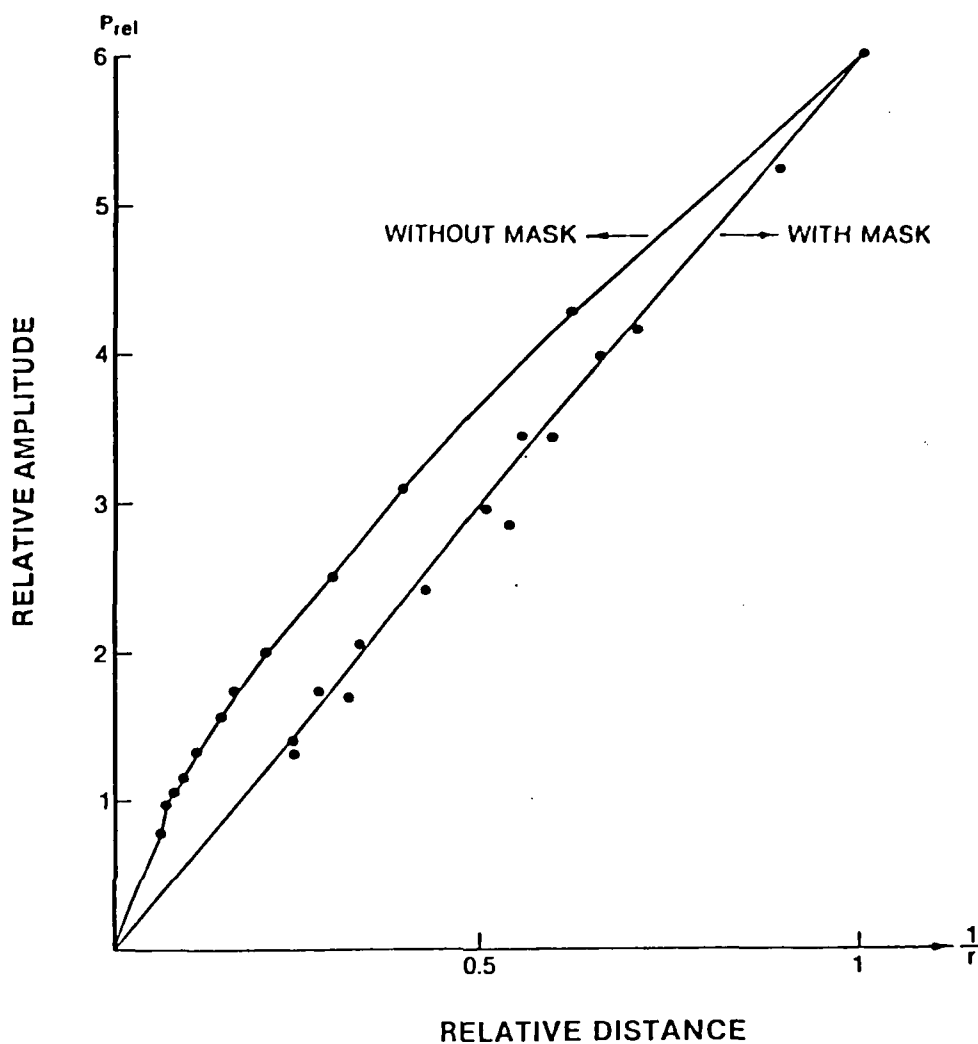
Figure 8. Radial Distance Relation of PA Signal from
Point Source With and Without Mask

the reference value. This procedure was found to be necessary because
of the gradual change in the PA signal with time. A point source with a
radius of 0.13 mm was used in this measurement, and the power density of
the Nd:YAG laser at the target surface was 1.16×10^9 W/cm^2.

Verification of Cylindrical Propagation of PA Signal

Although the masking effect is not critical in this measurement, an
aperture smaller than the length of the source was used to measure the

sound-propagation properties. In this experiment a 6.7 cm-long line source was formed by a cylindrical convex lens having a short focal length and several spherical convex and concave lenses. An adjustable aperture after the optical arrangement was used to ensure that a relatively uniform portion of the line was focused at the target. Because the power density of the line source was not intense, a coated aluminum plate, having a high absorption coefficient, was used as a target material. The same measurement procedure as that used for a point source was employed to determine the propagation properties.

The data are shown in Fig. 9. The reference point was set at 5.5 cm from the source. The power density of the pump laser at the target surface was about 1.0×10^6 W/cm^2. As shown in the figure, the agreement of the experimental data with the $1/\sqrt{r}$ relationship is good. Since a line source can be considered as a point source at very large radial distances, the amplitude relation gradually changes to $1/r$ at large distances. In this experiment, the PA signal propagated as a cylindrical wave to approximately six times the length of the source (i.e., 33 cm), where it diverged into a spherical wave. The transition appeared to be a function of the length and the power of the source.

Although the results are not presented in this thesis, a very short line source with high power density was studied in the same manner. The results showed the PA signal to propagate cylindrically to more than 15 times the length of the source. The propagation dependence of a cylindrical wave on the pump laser power and the length of the source was not examined in detail in this research and remains for future investigations.
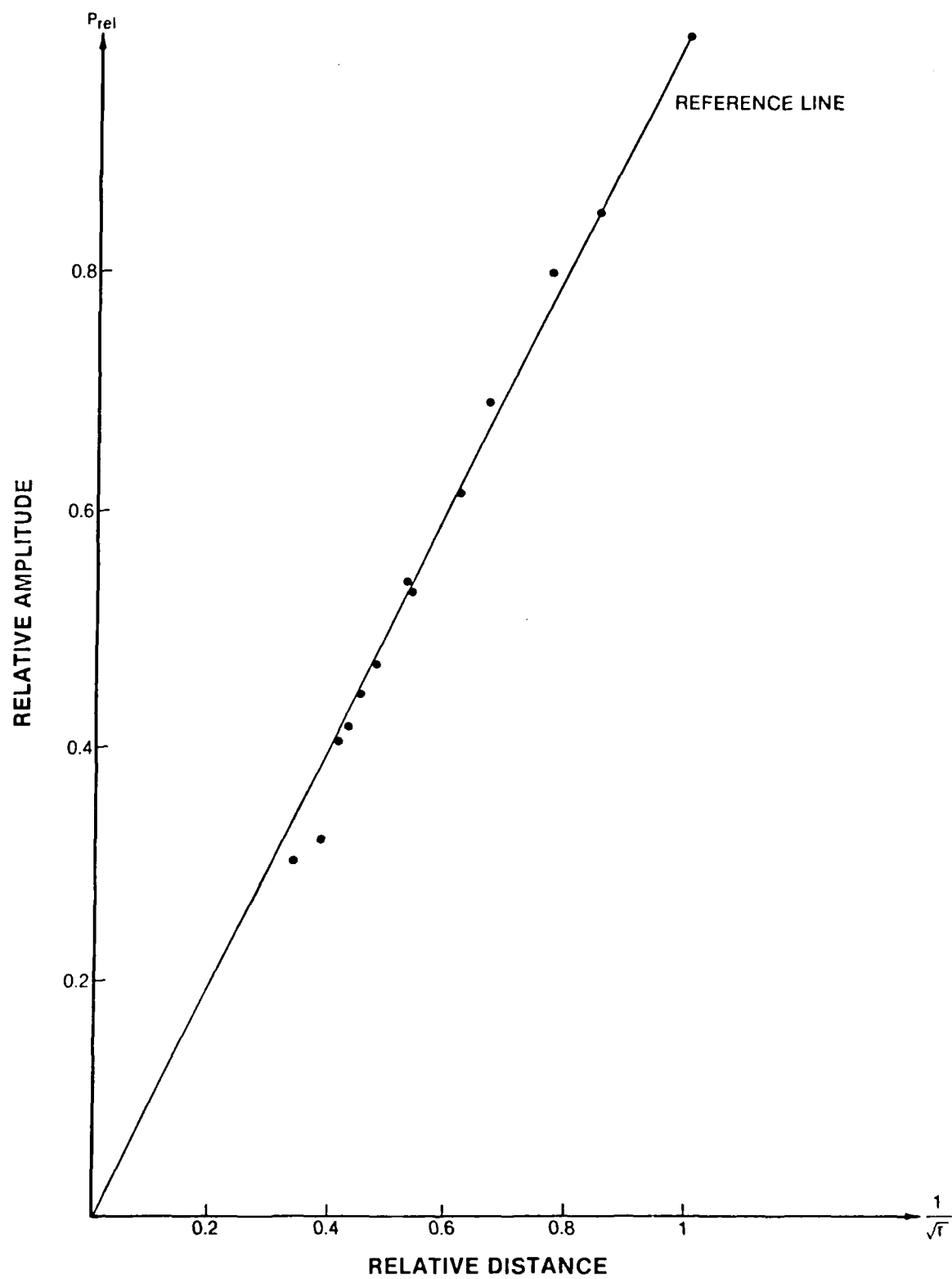
Figure 9. Cylindrical Propagation of PA Signal

37

Lateral Amplitude Distribution

The lateral amplitude distributions of the PA signals from a point and from several line sources were examined to determine their divergences. This measurement was made for a point source and several line sources having different lengths and power densities.

Point Source. The lateral amplitude distribution of the PA signal from a point source having a radius of 0.13 mm and a power density of 1.16×10^9 W/cm^2 is illustrated in Fig. 10. The distribution was measured at radial distances of 14 and 29 cm. At 14 cm the amplitude of the PA signal was reduced to one-half of the peak amplitude at a lateral distance of 2.75 cm from the center for each side. If one considers a half-width half-maximum (HWHM) region to be a sound width, the divergence angle is calculated to be 12°. At 29 cm the HWHM occurred at 5.5 cm for each side, and the divergence angle was about 11°. These measurements indicate that the point source radiates sound in a conical shape.

Cylindrical Signal. Several lengths of line sources were investigated using different power densities to determine the lateral amplitude distributions and divergence angles. The results are shown in Fig. 11. The divergence angles were calculated from the following equation:

$$\tan^{-1} \left(\frac{W - L}{2R} \right) \tag{50}$$

where W is the full-width half-maximum (FWHM) of the amplitude, L is the source length, and R is the radial distance from the source. The divergence angles were calculated using this equation and are shown in Table V for each line source.

38
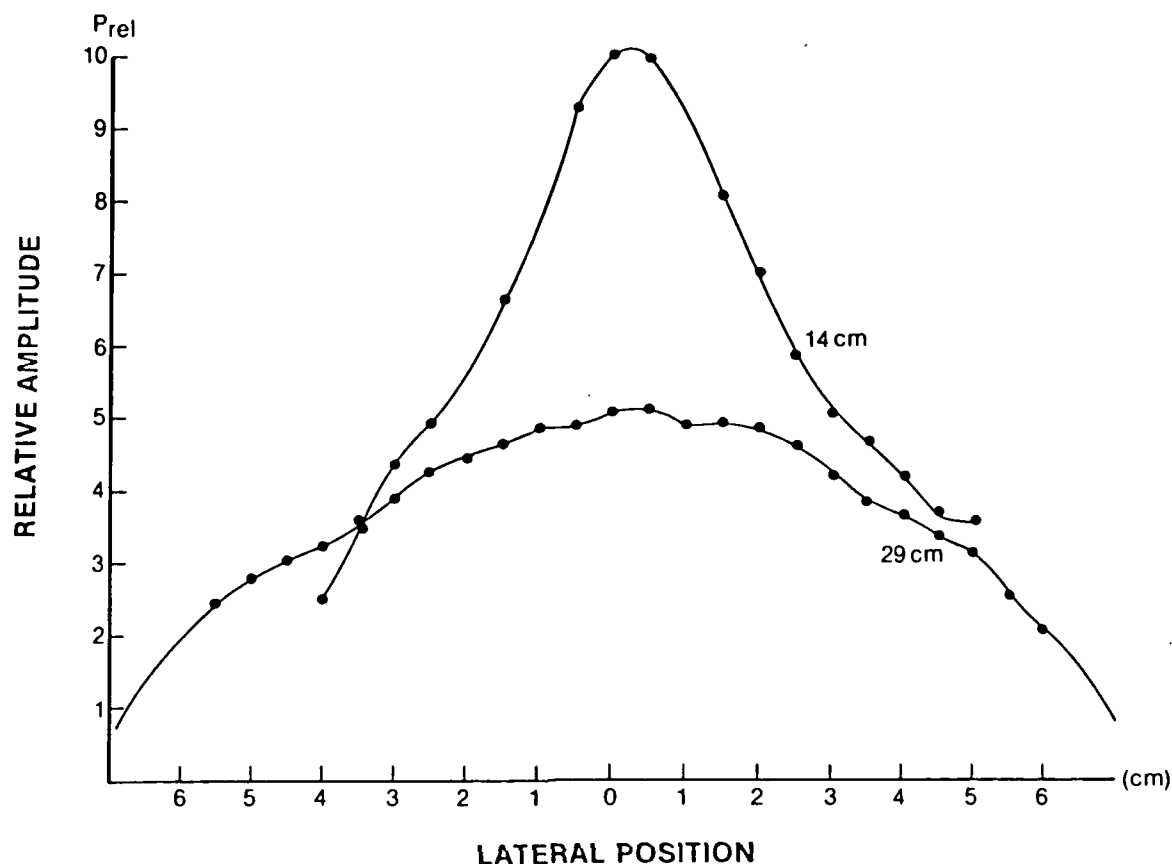
Figure 10. Lateral Amplitude Distribution of Spherical PA Signal

According to these data, when the power density and the source length are large, the divergence angle is small. The divergence angle was measured to be about 4°, which is much smaller than the point source (about 11°). If the source is more intense and uniform, one can expect the divergence angle to be less than 1°. The sound profiles shown in Fig. 11 are not completely uniform because of the laser beam profile of the unstable resonator pump source.
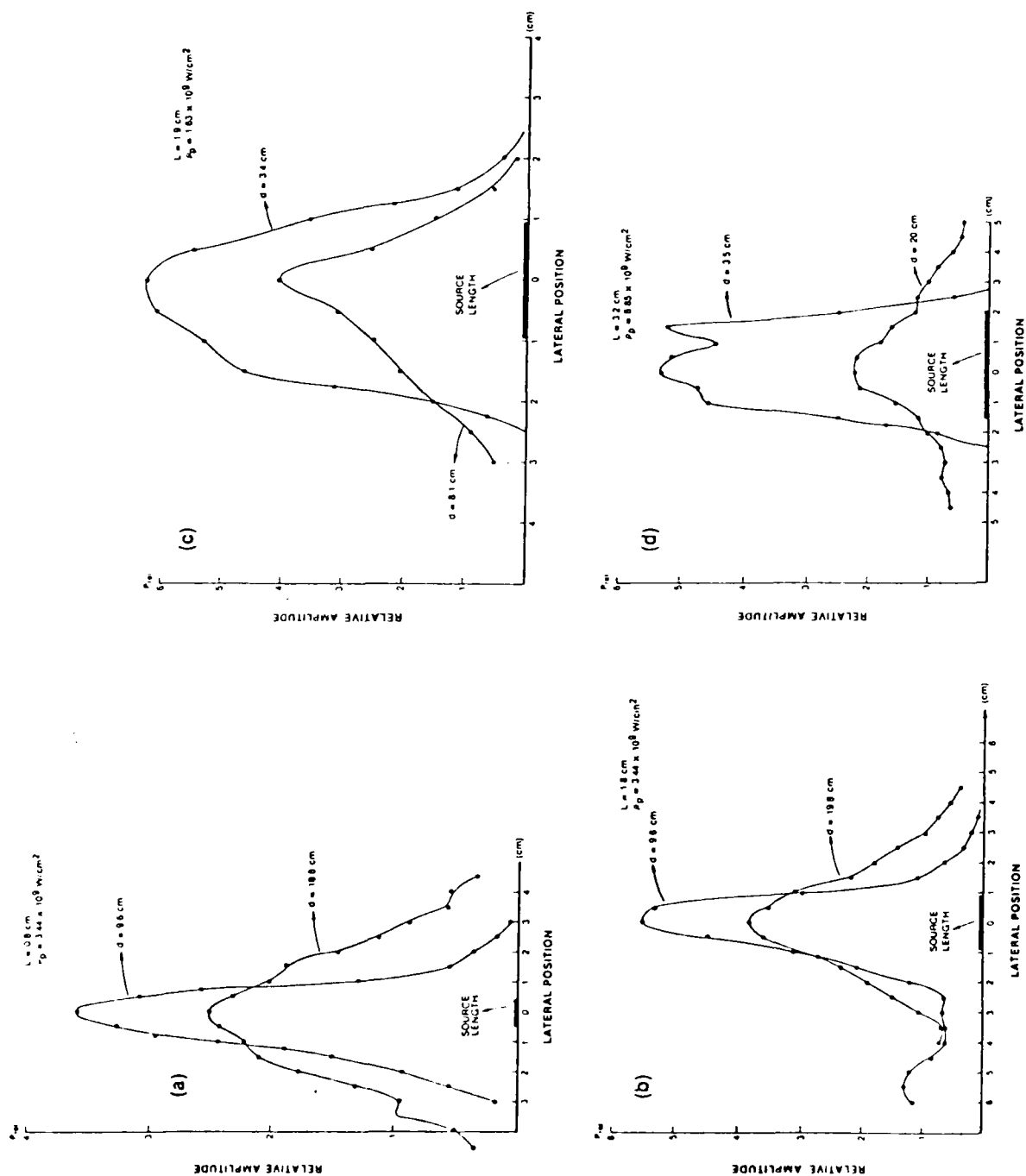
Figure 11. Lateral Amplitude Distributions of Cylindrical PA Signals
(L – Source Length, ρ_p – Power Density of Source)

TABLE V

Divergence Angles for Different Line Sources

Source Length	Radial Distance	Power Density	Divergence Angle
0.8 cm	9.6 cm	3.44×10^{11} W/cm^2	4.17°
	19.8 cm	"	5.77°
1.8 cm	9.6 cm	"	1.04°
	19.8 cm	"	3.6°
1.9 cm	3.4 cm	1.63×10^{11} W/cm^2	7.95°
	8.1 cm	"	3.88°
3.2 cm	3.5 cm	8.85×10^7 W/cm^2	2.68°
	20 cm	"	1.86°

Verification of Pump-Laser Power Dependence

The amplitudes of the PA signals were measured as a function of the Nd:YAG laser power. The results are shown in Fig. 12. The amplitude of the PA signal generated from a steel target varies linearly with the pump-laser power up to a power density of about 1.1×10^8 W/cm^2, and then flattens out due to saturation. In this experiment, the power density was varied up to 2.6×10^8 W/cm^2, and little increase was observed in the amplitude of the PA signal beyond saturation.

Figure 12. Sound Amplitude vs. Power Density

Comparison of the Amplitudes of PA Signals
Generated by Different Target Materials

The amplitudes of the sound pulses were measured along with the
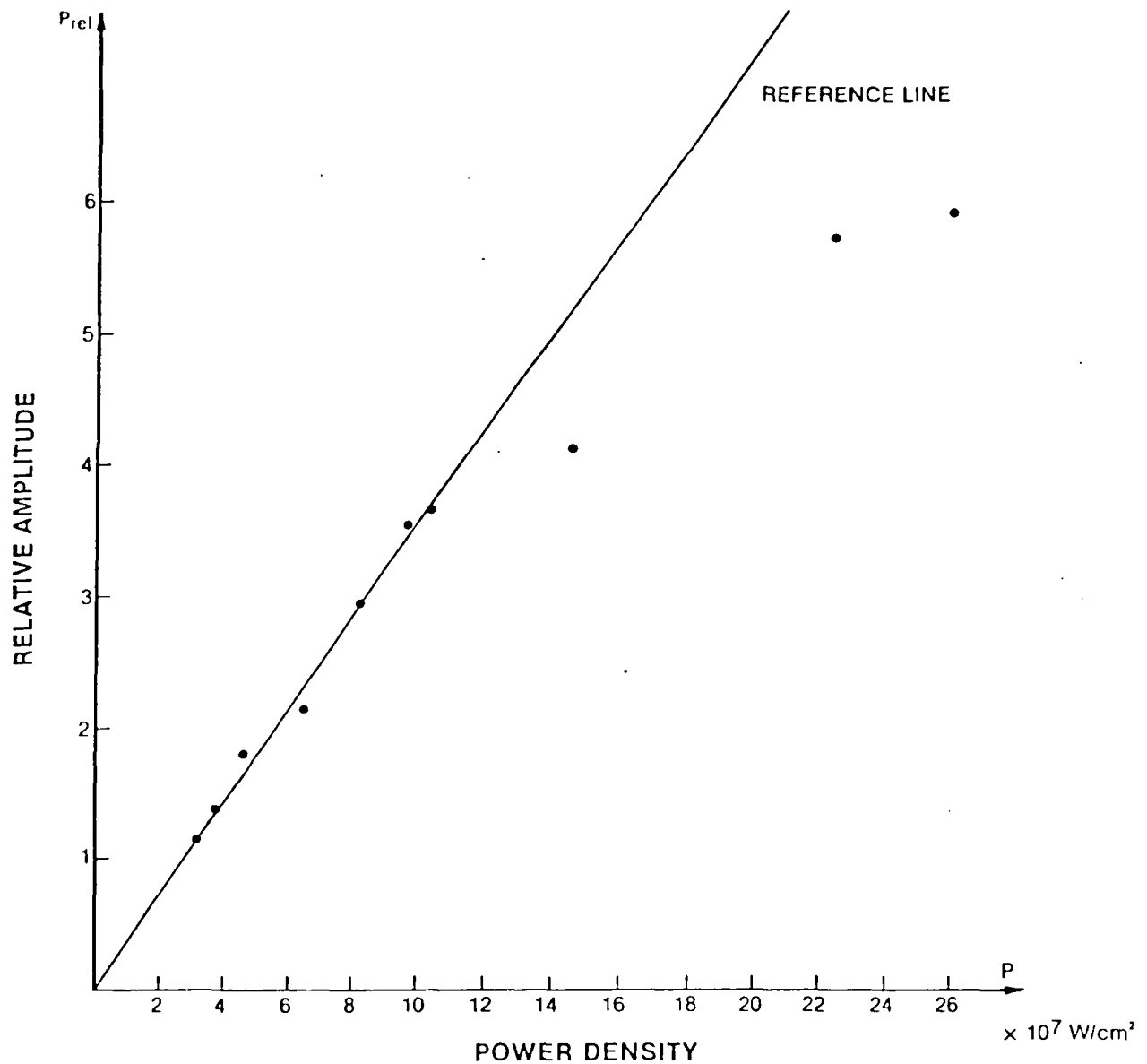time response for various target materials. This experiment was

42

performed with various pumping geometries, i.e., the target was placed slightly behind the focus, in front of the focus, and far in front of the focus.

Target Placed Slightly Behind Focus. The main purpose of this geometry was to investigate the plasma-generating properties of the target materials (42:213-275). When an intense laser pulse is absorbed on the surface of a solid, the resulting temperature rise at the surface can be sufficiently large to ionize the surrounding air. This phenomenon, which appears as a bright blue-white plasma close to the target surface (see Fig. 13), was not studied in detail here; however, several good plasma-generating materials were found, and the effect of the spark was examined by comparing the average amplitude of the sound generated with a spark and that generated without a spark. The data of this experiment are shown in Fig. 14. Stainless steel was found to be the best and most consistent sound-generating material. Nevertheless, the sound generated by titanium was stronger, although these data are plotted in the middle range of the figure. The reason for this is that the titanium generated a significant plasma spark which reduced the laser power density at the surface due to the broadband absorption of the plasma spark; thus, the average sound amplitude was smaller than that in many other materials.

The stainless-steel target consistently generated very strong sound without plasma sparks. The aluminum target generated the strongest sound for the first minute but melted easily and was etched by the pump laser beam; therefore, the sound amplitude degraded rapidly after the first few minutes.

A titanium alloy (90% titanium, 6% aluminum, and 4% tantalum) was used as a target and generated strong but inconsistent sound. The sound

43

(a)

(b)

Figure 13. Plasma Spark Generation by Titanium; (a) No Spark
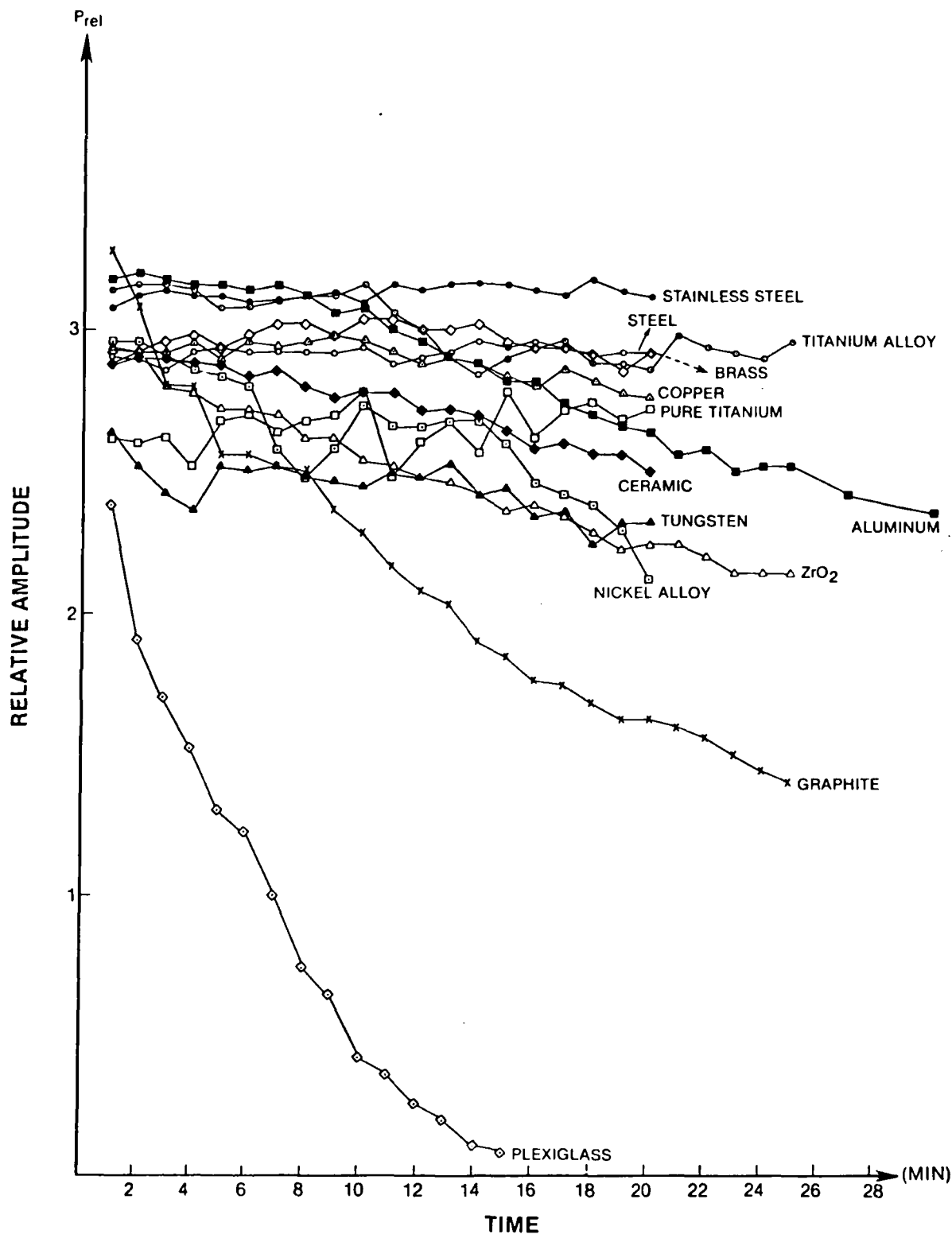Generated, (b) Spark Generated at Center of Picture

Figure 14.   Sound Amplitude Variation for Materials
Located Slightly Behind the Focus

45

generated by the titanium alloy was very unreliable. Brass, which is 70% copper and 30% zinc, was also a good sound-generating source. It often generated plasma sparks, however. Copper yielded nearly the same results as brass but was etched slightly faster than brass and the sound amplitude decreased after about 10 min. of exposure to the laser beam. An interesting observation was that tungsten generated rather weak sound and was etched easily. A ceramic was also used as a target material. It generated about the same amplitude of sound as brass, but the sound level decreased gradually. The sound generated from the nickel alloy was very unstable, as shown in Fig. 14. Some other non-metallic materials were examined, but they were etched very rapidly. The power density of the pump laser at the target surface in this experiment was 1.16 $\times$ 10^9 W/cm^2.

Target Placed in Front of Focus. In this experiment sound generated by materials without a plasma spark was examined, and the best sound-generating material was determined. The results are shown in Fig. 15. As noted previously pure titanium was determined to be the best sound-generating material. Steel and stainless steel yielded the same results as in the previous experiment. Brass and copper were also good and consistent target materials, but the amplitudes of the sounds generated by them are smaller than those from steel or stainless steel. Tungsten was concluded to be a poor target material. The power density of the pump laser used at the target surface was about 3 $\times$ 10^8 W/cm^2 .

Target Placed Far in Front of Focus. In this case, the target was placed far from the focus, where the radius of the beam spot was 0.71 mm and the power density was 2.37 $\times$ 10^7 W/cm^2. From Eq. (10), the
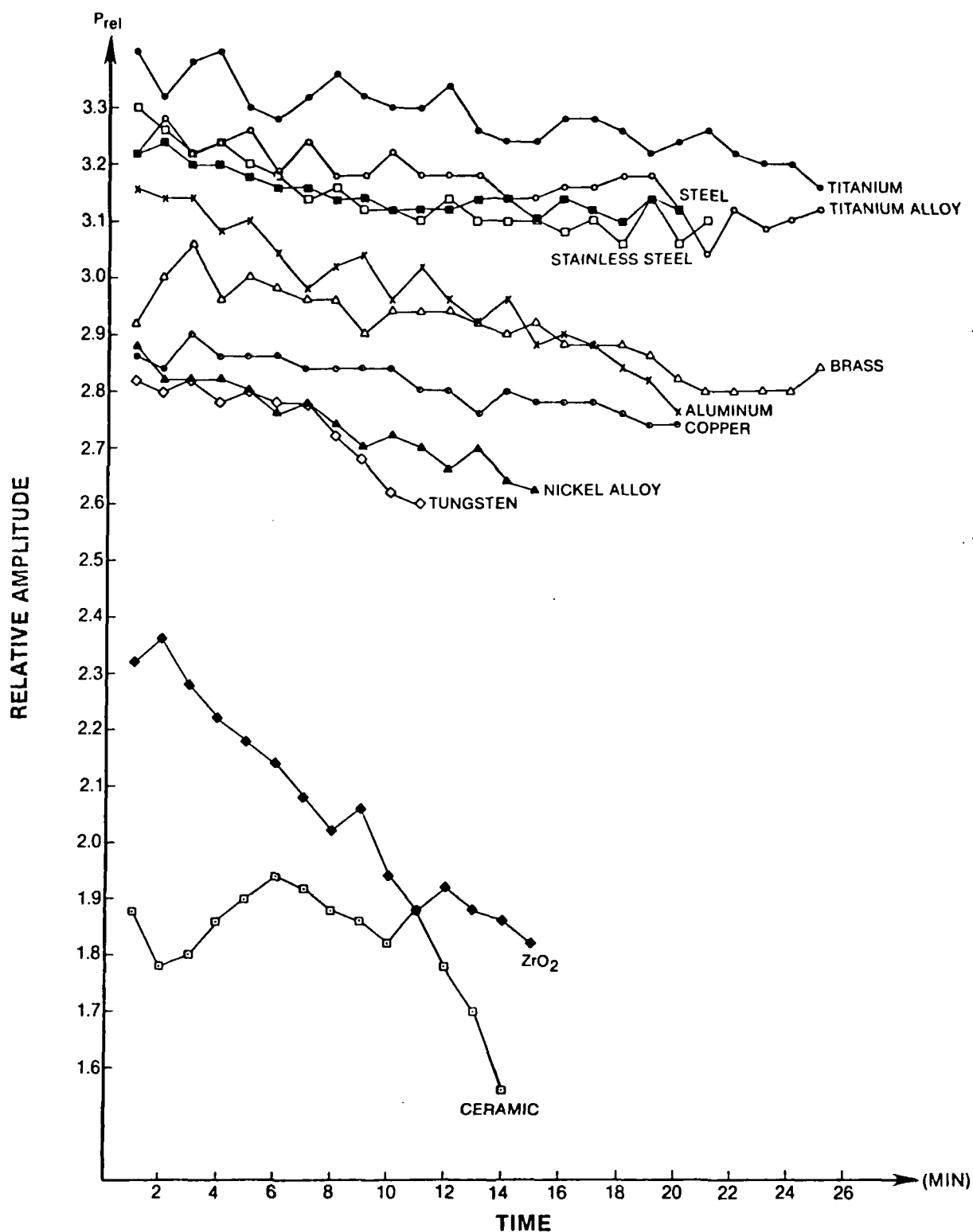
46

Figure 15. Sound Amplitude Variation for Materials
Located in Front of Focus

47

temperature rise ΔT at the surface was about $16^{\circ}C$ for steel, when the absorption coefficient of steel was assumed to be one.

Very interesting results were obtained in this experiment, as shown in Fig. 16. Titanium and titanium alloy generated the strongest sounds even in this case. The amplitude of the sound did not decrease but increased gradually and was fairly consistent. For steel and stainless steel, the amplitude of the PA signal increased for the first 13 min., decreased very rapidly after 19 min., and then increased again after 23 min. For aluminum, the sound amplitude increased very rapidly for the first 3 min. and then decreased very rapidly. Brass generated nearly the same amplitude-variation pattern as in the well-focused case. For nickel and copper the amplitudes increased gradually until they reached almost three times the intensity observed during first 1 min. The basis for these results was not treated in this research and remains for future studies.

Dependence of PA Signal upon Absorption Coefficient and Specific Heat. A change in material means a change in the absorption coefficient and the specific heat of the target. These parameters could not be examined separately in this study. The sound amplitude for each material is related to the ratio of the absorption coefficient to the specific heat of the material. The absorption coefficients and specific heats for the materials employed in this experiment are listed in Table VI. Since the absorption coefficients at the frequency of the Nd:YAG laser (1.064 μm) were not obtainable, those of solar radiation were used in this table. However, even the absorption coefficients for solar radiation were not sufficiently known. The thermal conductivity was listed in the table to relate the amplitude of the PA signal to the

48
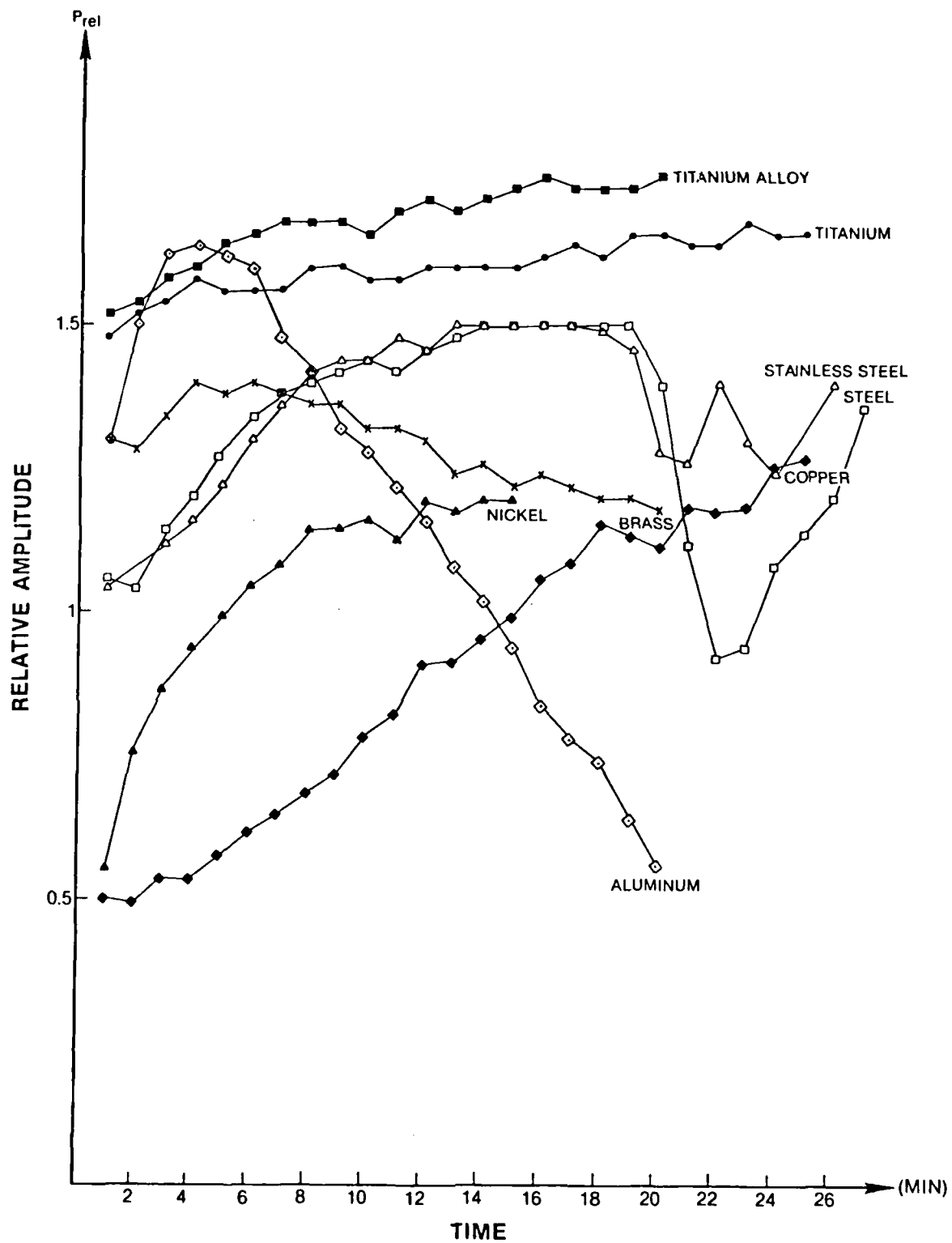
Figure 16.   Sound Amplitude Variation for Materials
Located Far in Front of the Focus

49

Table VI

Absorption Coefficients, Specific Heats, Thermal Conductivities, and Generated Sound Amplitudes
(From CRC Handbook of Chemistry and Physics)

Contents / Materials	ⓐ Absorption Coefficient	ⓑ Specific Heat (Cal/g)	Thermal Conductivity (W/cm K)	ⓐ/ⓑ	Sound Amplitude for Well Focused Case	Sound Amplitude for Mildly Focused Case
Titanium		0.1248	0.21		3.4	1.48
Titanium Alloy		0.1266	0.363		3.22	1.52
Steel	0.20	0.1075	0.82	1.86	3.22	1.06
Stainless Steel		0.108			3.3	1.04
Aluminum	0.15	0.215	2.36	0.698	3.16	1.3
Copper	0.25	0.0924	4.0	2.706	2.86	0.5
Brass	0.34	0.0923	3.16	3.68	2.92	1.3
Nickel	0.15	0.1061	0.9	1.414	2.88	0.55
Tungsten		0.0322	1.7		2.82	~0
Zirconium		0.0660	0.21		1.88	~0

thermal conductivity. According to the Patel-Tam model, the lower the thermal conductivity, the larger the sound amplitude for a given pump power density. The sound amplitude listed in the table is the average value for the first minute; therefore, it differs slightly from the amplitude of the sound without melting and surface-variation effects.

For the well-focused case, the amplitude of the sound is different from that expected due to the saturation effect. The first PA signals produced in the mildly focused case during the first minutes provide a better source of comparison for the absorption coefficients and the specific heats. However, the sound amplitude could not be related to the ratio of absorption coefficient to specific heat. It is believed that these results were obtained for the following reasons: 1) the absorption coefficients for solar radiation are different from those for the Nd:YAG beam, 2) the surface conditions of the targets were not the same, and 3) the pump laser beam intensity was not uniform.

For high power density, which is more useful in practical applications, the sound generation depended not only upon the absorption coefficient and the specific heat but also upon other properties such as melting point, annealing, temperature, stress, and surface conditions.

VI. Summary

The purpose of this study was to investigate the characteristics of photoacoustic signals generated at the surface of condensed matter. The dependence of the peak pressure of the photoacoustic signal upon the radial distance and the pump-laser power level was determined and compared to the model of Patel and Tam.

The results of this study indicate that the dependence of the peak pressure upon radial distance and pump-laser power level agrees with the predicted dependence of the model of Patel and Tam. However, deviations from this model can occur for cylindrical waves at large radial distances.

The lateral sound-amplitude distributions were examined. From these results the divergence angles of cylindrical and spherical waves were calculated. Because of the lower radial divergence of a cylindrical wave as compared to a spherical wave, the line source appears to be better suited to practical applications such as non-contact flame temperature measurements. Through investigation of the sound amplitudes generated at the surfaces of numerous samples, the optimum sound-generating material (titanium) was found.

The model of the peak pressure of photoacoustic signals was not fully verified due to the limitations of the experimental apparatus and the lack of absorption coefficients of the materials at the pump-laser frequency.

Bibliography

1. Rosencwaig, A. "Photoacoustic Spectroscopy of Solids," Optics Communications, 7: 305-308 (1973).

2. Rosencwaig, A. "Photoacoustic Spectroscopy of Biological Materials," Science, 181: 657-658 (1973).

3. Rosencwaig, A. and S. S. Hall. "Thin-Layer Chromotography and Photoacoustic Spectrometry," Analytical Chemistry, 47: 548-549 (1975).

4. Rosencwaig, A. "Photoacoustic Spectroscopy (A New Tool for Investigation of Solids)," Analytical Chemistry, 47: 592A-604A (1975).

5. Hordvik, A. "Measurment Technique for Small Absorption Coefficient: Recent Advances," Applied Optics, 16: 2827-2833 (1977).

6. Hordvik, A. and H. Schlossberg. "Photoacoustic Technique for Determining Optical Absorption Coefficients in Solids," Applied Optics, 16: 101-107 (1977).

7. Hordvik, A. and L. Skolnik. "Photoacoustic Measurements of Surface and Bulk Absorption in HF/DF Laser Window Materials," Applied Optics, 16: 2919-2924 (1977).

8. Robin, M. B. "Direct Measurements of Radiationless Transitions in Molecules and Crystals," Journal of Luminescence, 13: 131-138 (1976).

9. Robin, M. B. and N. A. Kuebler. "Radiationless Decay in Aromatic Ketones as Studied by Opto-Acoustic Spectroscopy," American Chemical Society Journal, 97: 4822-4825 (1975).

10. Rosencwaig, A. "Photoacoustic Spectroscopy of Solids," Review of Scientific Instruments, 48: 1133-1137 (1977).

11. Rosencwaig, A. and A. Gersho. "Theory of the Photoacoustic Effect with Solids," Journal of Applied Physics, 47: 64-69 (1976).

12. Samoano, R. B. "Photoacoustic Spectroscopy of Condensed Matter," Angewandt Chemie International Edition in English, 17: 238-245 (1978).

13. Pao, Y. H. Optoacoustic Spectroscopy and Detection. New York: Academic Press, 1977.

14. Aamodt, L. C., J. C. Murphy, and J. G. Parker. "Size Considerations in the Design of Cells for Photoacoustic Spectroscopy," Journal of Applied Physics, 48: 927-933 (1977).

15. Aamodt, L. C. and J. C. Murphy. "Photoacoustic Spectroscopy of Luminescent Solids: Ruby," Journal of Applied Physics, 48: 3502-3509 (1977).

16. Aamodt, L. C. and J. C. Murphy. "Size Considerations in the Design of Cells for Photoacoustic Spectroscopy. II. Pulsed Excitation Response," Journal of Applied Physics, 49: 3036-3045 (1978).

17. McDonald, F. A. and G. C. Wetsel, Jr. "Generalized Theory of the Photoacoustic Effect," Journal of Applied Physics, 49: 2313-2322 (1978).

18. Patel, C. K. N. and A. C. Tam. "Optoacoustic Spectroscopy of Liquids," Applied Physics Letters, 34: 467-470 (1979).

19. Allen, Jr. J. E., W. R. Anderson, and D. R. Crosley. "Optoacoustic Pulses in a Flame," Optics Letters, 1: 118-120 (1977).

20. Tennal, K., G. J. Salamo, and R. Gupta. "Minority Species Concentration Measurements in Flames by the Photoacoustic Technique," Applied Optics, 21: 2133-2140 (1982).

21. Rose, A., G. J. Salamo, and R. Gupta. "Photoacoustic-Deflection Spectroscopy: A New Specie-Specific Method for Combustion Diagnostics," Applied Optics, 23(6): 781-784 (March 15, 1984).

22. Rose, A., J. D. Pyrum, C. Muzny, G. J. Salamo, and R. Gupta. "Application of the Photothermal Deflection Technique to Combustion Diagnostics," Applied Optics, 21: 2663-2665 (1982).

23. Jackson, W. B., N. M. Amer, A. C. Boccara, and D. Fournier. "Photothermal Deflection Spectroscopy and Detection," Applied Optics, 20: 1333-1344 (1981).

24. Zapka, W., P. Pokrowsky, and A. C. Tam. "Noncontact Optoacoustic Monitoring of Flame Temperature Profiles," Optics Letters, 7: 477-479 (1982).

25. Kizirnis, S. W., R. J. Brecha, B. N. Ganguly, L. P. Goss, and R. Gupta. "Hydroxyl (OH) Distribution and Temperature Profiles in a Premixed Propane Flame Obtained by Laser Deflection Techniques," Applied Optics, 23: 3873-3881 (1984).

26. Patel, C. K. N. and A. C. Tam. "Pulsed Optoacoustic Spectroscopy of Condensed Matter," Revised Modern Physics, 53: 517-550 (1981).

27. Askaryan, G. A., A. M. Prokhorov, G. F. Chanturiya, and G. P. Shipulo. "The Effects of a Laser Beam in a Liquid," Soviet Physics (JETP), 17: 1463-1465 (1963).

28. Bell, C. E. and J. A. Landt. "Laser-Induced High-Pressure Shock Waves in Water," Applied Physics Letters, 10: 46-48 (1967).

29. Bushanam, G. S. and F. S. Barnes. "Laser-Generated Thermoelastic Shock Wave in Liquids," Journal of Applied Physics, 46: 2074-2082 (1975).

30. Emmony, D. C., M. Siegrist, and F. K. Kneubühl. "Laser-Induced Shock Waves in Liquids," Applied Physics Letters, 29: 547-549 (1976).

31. Gordienko, V. M., A. B. Reshilov, and V. I. Shmal'gauzen. "Strobo-scopic Observation of Optoacoustic Interactions," Soviet Physics (Acoustics), 24: 73-74 (1978).

32. Gournay, L. S. "Conversion of Electromagnetic to Acoustic Energy by Surface Heating," Acoustical Society of America Journal, 40: 1322-1330 (1966).

33. Von Gutfeld, R. J. and H. F. Budd. "Laser-Generated MHz Elastic Waves from Metallic-Liquid Interfaces," Applied Physics Letters, 34: 617-619 (1979).

34. Sigrist, M. W. and F. K. Kneubühl. "Laser-Generated Stress Waves in Liquids," Acoustical Society of America Journal, 64: 1652-1663 (1978).

35. White, R. M. "Generation of Elastic Waves by Transient Surface Heat-ing," Journal of Applied Physics, 34: 3559-3567 (1963).

36. Kohanzadeh, Y., J. R. Whinnery, and M. M. Carroll. "Thermoelastic Waves Generated by Laser Beams of Low Power," Acoustical Society of America Journal, 57: 67-71 (1975).

37. Naugol'nykh, K. A. "Acoustooptical Pulse Phenomena," Soviet Physics (Acoustics), 23: 98-99 (1977).

38. Tam, A. C. and C. K. N. Patel. "Optical Absorptions of Light and Heavy Water by Laser Optoacoustic Spectroscopy," Applied Optics, 18: 3348-3358 (1979).

39. Landau, L. D. and E. M. Lifshitz. Fluid Mechanics (Translated from the Russian by J. B. Sykes and W. H. Reid). Reading, Massachusetts: Addison-Wesley Publishing Company, 1959.

40. Bunkin, F. V. and V. M. Komissarov. "Optical Excitation of Sound Waves," Soviet Physics (Acoustics), 19: 203-211 (1973).

41. Lyamshev, L. M. and K. A. Naugol'nykh. "Sound Generation by Thermal Sources," Soviet Physics (Acoustics), 22: 354-355 (1976).

42. Casperson, L. W. "Gaussian Light Beams in Inhomogeneous Media," Applied Optics, 12: 2434-2441 (1973).

43. Wolfe, W. L. and G. J. Zissis. Infrared Handbook. Washington, D. C.: Department of the Navy, 1978.

44. Ready, John F. Effects of High-Power Laser Radiation. New York: Academic Press, 1971.

VITA

Haksoo Yoon was born on March 20, 1955, in Seoul, Korea, and graduated from Choong-Ang Senior High School in 1973. He entered Korean Air Force Academy and graduated with a Bachelor of Science degree in electrical engineering. After graduation from the Korean Air Force Academy, he was trained as a fighter pilot for two years and was assigned to the 120th Fighter Squadron, 18th Fighter Wing of the Korean Air Force in April 1979. His second assignment was the Cadet Wing of the Korean Air Force Academy as an Air Officer Commanding. After one year of service in the Air Force Academy, he was re-assigned to the 18th Fighter Wing.

Haksoo Yoon entered the U. S. Air Force Institute of Technology in June 1983 and was promoted to major the next month.

<div style="text-align:right">

Permanent address: 218-33
Noryangjin-Dong
Tongjak-Gu
Seoul, 151
Korea

</div>

REPORT DOCUMENTATION PAGE

1a. REPORT SECURITY CLASSIFICATION UNCLASSIFIED		1b. RESTRICTIVE MARKINGS			
2a. SECURITY CLASSIFICATION AUTHORITY		3. DISTRIBUTION/AVAILABILITY OF REPORT Approved for public release; distribution unlimited			
2b. DECLASSIFICATION/DOWNGRADING SCHEDULE					
4. PERFORMING ORGANIZATION REPORT NUMBER(S) AFIT/GEO/PH/84D-6		5. MONITORING ORGANIZATION REPORT NUMBER(S)			
6a. NAME OF PERFORMING ORGANIZATION School of Engineering	6b. OFFICE SYMBOL (If applicable) AFIT/ENP	7a. NAME OF MONITORING ORGANIZATION			
6c. ADDRESS (City, State and ZIP Code) Air Force Institute of Technology Wright-Patterson Air Force Base, OH 45433		7b. ADDRESS (City, State and ZIP Code)			
8a. NAME OF FUNDING/SPONSORING ORGANIZATION Aero-propulsion Laboratory	8b. OFFICE SYMBOL (If applicable) AFWAL/POOC	9. PROCUREMENT INSTRUMENT IDENTIFICATION NUMBER			
8c. ADDRESS (City, State and ZIP Code) Wright-Patterson AFB, OH 45433		10. SOURCE OF FUNDING NOS.			

		PROGRAM ELEMENT NO.	PROJECT NO.	TASK NO.	WORK UNIT NO.
11. TITLE (Include Security Classification) See Box 19					

12. PERSONAL AUTHOR(S) Haksoo Yoon, B.S., Major, ROKAF				
13a. TYPE OF REPORT MS Thesis	13b. TIME COVERED FROM _____ TO _____	14. DATE OF REPORT (Yr., Mo., Day) 1984 December		15. PAGE COUNT 65

16. SUPPLEMENTARY NOTATION

17. COSATI CODES			18. SUBJECT TERMS (Continue on reverse if necessary and identify by block number)
FIELD	GROUP	SUB. GR.	Photoacoustics, Sound Propagation, Sound Generation.
20	01		

19. ABSTRACT (Continue on reverse if necessary and identify by block number)

Title: EXPERIMENTAL INVESTIGATION OF THE PULSED PHOTOACOUSTIC EFFECT PRODUCED ON A SOLID SURFACE

Thesis Advisor: Won B. Roh, Ph.D.

Approved for public release: IAW AFR 190-17.

LYNN E. WOLAVER ƚ/Feb 8ſ
Dean for Research and Professional Development
Air Force Institute of Technology (ATC)
Wright-Patterson AFB OH 45433

20. DISTRIBUTION/AVAILABILITY OF ABSTRACT UNCLASSIFIED/UNLIMITED ☒ SAME AS RPT. ☐ DTIC USERS ☐	21. ABSTRACT SECURITY CLASSIFICATION UNCLASSIFIED	
22a. NAME OF RESPONSIBLE INDIVIDUAL Won B. Roh, Ph.D.	22b. TELEPHONE NUMBER (Include Area Code) (513) 255-4498	22c. OFFICE SYMBOL AFIT/ENP

The purpose of this investigation was to determine the characteristics of the photoacoustic signal generated from the surface of a solid material. The important characteristics considered were the dependence of the signal upon 1) the pump-laser power level, 2) the absorption coefficient and specific heat of the material, 3) the radial and axial sound distribution, and 4) the distribution of sound with laser focal characteristics.

The model of peak sound pressure for the photoacoustic effect employed in this study was developed by Patel and Tam for liquids. The divergence angles of cylindrical and spherical sound waves were calculated by means of the lateral sound pressure distribution. The optimum sound-producing material was determined by investigating numerous material samples.

Throughout the study the peak pressure of the photoacoustic sound pulse was measured through the use of the linear deflection of a HeNe probe beam. The results of this investigation indicate that the Patel model for the peak pressure of a photoacoustic signal gives an adequate description of the dependence of the sound pressure upon radial distance and pump-laser power level. However, the dependence of the sound pressure upon the absorption coefficient and the specific heat of a material could not be verified due to the unavailability of absorption coefficients of the materials studied at the Nd:YAG laser frequency. The results of this study indicate that a cylindrical wave generated by titanium is optimum for applications to the measurement of flame temperatures. The dependence of the sound pressure upon the pump-laser pulse width was not studied.